# PERFORMANCE OF PVD COATINGS FOR MACHINING UNS S32750

# TRIBOLOGICAL AND WEAR PERFORMANCE OF PVD COATINGS FOR MACHINING SAF 2507 (UNS S32750) SUPER DUPLEX STAINLESS STEEL

By ANDRE BEPE, B.ENG., M.SC.

A Thesis submitted to the School of Graduate Studies in partial fulfilment of the requirements for the Degree of Master of Applied Science in Mechanical Engineering.

| | |
|---|---|
| Master of Applied Science (2023)<br>Department of Mechanical Engineering | McMaster University<br>Hamilton, Ontario, Canada |

TITLE: Tribological and wear performance of PVD coatings for machining SAF 2507 (UNS S32750) Super Duplex Stainless Steel

AUTHOR: Andre Mello Bepe

M.Sc. – Materials Sciences and Engineering (UNIFESP, Brazil)

B.Eng. – Chemical Engineering (UNIVAP, Brazil)

SUPERVISOR: Dr. Stephen Veldhuis

Department of Mechanical Engineering

McMaster University

NUMBER OF PAGES: xii,80

# LAY ABSTRACT

Super duplex stainless steels are designed to be applied in highly corrosive environments. Like any other stainless steels, processing the super duplex grade can be challenging, especially when it comes to machining. The major causes of poor machined surface quality and rapid tool wear are high temperature, the workpiece enhanced mechanical properties, surface hardening and the tendency to stick to the cutting tool causing adhesive wear. This research explores the application of coated cutting tools to improve the machinability of the super duplex stainless steel UNS S32750. Different commercially available coatings were tested and two, Alcronos and Alnova, improved tool life significantly. These two coatings were capable of improving the friction conditions within the cutting zone which, in turn, helps with the formation of the chips and leads to a better machined surface integrity and an approximately 5 to 6 times longer tool life.

# ABSTRACT

Super duplex stainless steels are applied in highly corrosive environments. To withstand such conditions, they designed with increased content of alloying elements and a duplex microstructure consisting of austenitic and ferritic phases. The result of this combination is the desired improvement in corrosion resistance, but also, the enhancement of mechanical properties. Machining super duplex stainless steels involves strain hardening of the workpiece, intense adhesive wear and elevated temperatures within the cutting zone leading to rapid tool wear and poor machined surface integrity. This research pertains to the application of commercially available PVD coatings to minimize the detrimental effects when turning super duplex stainless steel S32750. The selected coatings for this study were Alcronos (AlCrN), Alnova (AlCrN + AlCrSiN), Formera (CrN + CrAlTiN), Croma Plus (Cr + CrN + OX), Fortiphy (CrN) and Certiphy (TiAlN). The wear behavior and mechanisms in two distinct machining experiments were evaluated, and all tools failed by chipping preceded by intense adhesive wear and BUE formation. The use of AlCrN coatings improved tool life significantly. Data on the cutting force, chip formation, and workpiece surface integrity indicate less workpiece strain hardening effects, improved friction conditions at the tool/chip interface, as well as thinner chips being formed when machining with Alcronos coated carbide inserts. The micro-mechanical properties of the selected coatings were assessed and Alcronos combined high hardness and elastic modulus with a high plasticity index value that allows this coating to better manage the friction in the cutting zone and better dissipate the energy generated during cutting.

# ACKNOWLEDGEMENT

I extend my deepest gratitude to Dr. Stephen Veldhuis for the opportunity given to me. Joining the McMaster Manufacturing Research Institute team not only provided me with invaluable opportunities but also equipped me with the necessary resources to undertake and complete this research successfully.

I am deeply grateful to Dr. Jose Mario De Paiva for his unwavering guidance, friendship, and encouragement throughout the Master's program. Additionally, I extend my heartfelt thanks to Dr. Qianxi He and Dr. Monica Costa Rodrigues Guimaraes for their indispensable support in conducting various characterization experiments. Their expertise was crucial for the realization of this research.

Special gratitude is extended to my wife, Aline, whose unwavering love and support served as a pillar during the demanding journey of my Master's program. Her resilience and emotional support were indispensable, holding our family together during the most challenging times.

I am also thankful to my mother, Berenice, and my father, Nassibe, for their life examples and for instilling in me the qualities of resilience that have been fundamental in my academic pursuits. To my son, Victor, and my daughter, Livia, I am grateful for being a constant source of inspiration, making me a better person each day.


The most beautiful thing we can experience is the mysterious.

It is the source of all true art and science.

Albert Einstein

# CONTENTS

# LIST OF FIGURES

# LIST OF TABLES

# NOTATIONS AND ABBREVIATIONS

DSS – Duplex Stainless Steel

SDSS – Super Duplex Stainless Steel

UNS – Unified Numbering System

$PRE_N$ – Pitting Resistance Equivalent Number

PSDZ – Primary Shear Deformation Zone

SSDZ – Secondary Shear Deformation Zone

TSDZ – Tertiary Shear Deformation

BUE – Build Up Edge

PVD – Physical Vapor Deposition

CVD – Chemical Vapor Deposition

TiAlN – Titanium Aluminum Nitride

AlCrN – Aluminum Chromium Nitride

CrN – Chromium Nitride

HiPIMS - High Power Impulse Magnetron Sputtering

SEM – Scanning Electron Microscopy

EDS – Energy-dispersive Spectroscopy

XRD – X-ray Diffraction

E – Elastic Modulus

H – Hardness

PI – Plasticity Index

# 1. INTRODUCTION

## 1.1. Research Background and Motivation

The development of new technologies is the main driving force for the advancement of modern society. Industries are constantly and fiercely seeking to improve their products and to introduce innovative solutions. Within this dynamic market, the demand for advanced materials is escalating. The stainless steels are among these materials, and since their discovery, they have been used in countless applications. The development of stainless steels is closely connected to the advances in many, if not all, industry sectors (1). Different types of stainless steels are available in the market to address several challenges related to corrosion and oxidation. Ferritic, austenitic, and martensitic stainless-steel grades were first introduced and revolutionized many industrial processes and products. As research intensified, driven by the need for more advanced materials, duplex and super duplex grades were created (2).

Processing stainless steels can be a daunting task for manufacturers. As an example, in machining processes (turning, milling, drilling, etc.), these materials are considered difficult to cut due to their improved properties. The S32750 super duplex stainless steel, with increased content of chromium and alloying elements such as Mo and Ni has an outstanding corrosion resistance combined with higher mechanical and physical properties, making it an ideal candidate to replace the other stainless-steel grades in several applications. However, when processing S32750 through machining operations, extreme

conditions are expected to be generated within the cutting zone, which lead to premature tool failure and excessive production costs related to tooling and machine downtime (3,4).

One major challenge related to machining stainless steels is the built-up edge (BUE) formation. The microstructural and mechanical properties of S32750 favor the accumulation of workpiece material on the edge of the cutting tool. Layer after layer of work hardened stainless steel gradually builds up changing the shape of the cutting edge and affecting heat generation, surface integrity, cutting forces and tool integrity. When cutting S32750 the main tool wear mechanisms expected are adhesion and chipping that are further aggravated by high temperature and oxidation (5).

To minimize and overcome these problems, manufacturers can benefit from the use of coated carbide tools that offer extended tool life and, therefore, a reduction in the previously mentioned expenses. Titanium-based PVD coatings such as TiN, TiCN, TiAlN, have been successful in this regard (6). While these coatings are well established in the market due to their versatility and proven benefits, the use of chromium based PVD coated cutting tools for machining such grade of stainless steel may offer an alternative. Cr, being the hardest pure metal is an excellent candidate for hard coatings, especially when combined with aluminum in Al-Cr coatings. Under high temperature and pressure, both Al and Cr may react with oxygen forming nanometric ceramic tribofilms that act as a thermal insulation, as well as a wear protective layer (7,8). These types of coatings can offer enhanced protection for cutting tools that are submitted to harsh machining conditions typical to the machining of S32750 super duplex stainless steels.

## 1.2. Research Objectives

Based on the literature review, the behavior of Cr based PVD coatings for machining S32750 super duplex stainless steel can be further investigated. This research intends to contribute to the study of the wear performance of commercially available Cr based PVD coatings deposited on carbide cutting inserts for finish turning of S32750. The following coatings were selected:

| Manufacturer | Commercial Name | Composition | Deposition method |
|---|---|---|---|
| **Oerlikon** | **Formera** | **CrN + CrAlTiN** | **Arc** |
| **Oerlikon** | **Alcronos** | **AlCrN** | **HiPIMS** |
| **Oerlikon** | **Alnova** | **AlCrN + AlCrSiN** | **Arc** |
| **Oerlikon** | **Croma Plus** | **Cr + CrN + OX** | **Arc** |
| **Oerlikon** | **Alcrona Pro** | **AlCrN** | **Arc** |
| **Phygen** | **Fortiphy** | **CrN** | **HiPIMS** |
| **Phygen** | **Certiphy** | **TiAlN** | **HiPIMS** |

The TiAlN coating was selected as an industry standard for Ti-based coatings.

To complete this investigation the following objectives were determined:

1. The study of the mechanical and tribological properties, morphology and chemical composition of the proposed coatings.
2. The evaluation of the cutting tool life and wear mechanisms for finish turning of S32750 through controlled machining experiments.
3. The analysis of the integrity of machined surface and chip formation.

## 1.3. Thesis Outline

The content of this research work was divided into six chapters:

1. INTRODUCTION

The first chapter explores the motivation and main goals that underly this research.

2. LITERATURE REVIEW

Contains the theoretical background and relevant references that support the development of the experimental procedure and provides sufficient knowledge to examine the findings of this work. The three major topics that are addressed in this chapter are:

- Duplex Stainless Steels
- Machining and Cutting Tools
- Coatings for Cutting Tools.

3. EXPERIMENTAL PROCEDURE

This chapter defines the methodology employed in this study, the equipment used, as well as the experimental setups and characterization techniques. It is subdivided into:

- Tool Wear Performance Tests
- Coating Characterization

4. RESULTS AND DISCUSSIONS

Presents the outcomes of the experiments and analyses, including an in-depth discussion of these findings and comments about similar relevant research works, that either support or contradict this study's results.

5. CONCLUSIONS

The major conclusions and contributions of this work to the existing knowledge are stated in this Chapter.

6. SUGGESTIONS FOR FURE WORK

The last chapter includes recommendations for further studies related to this project.

# 2. LITERATURE REVIEW

## 2.1. Duplex Stainless Steels

### 2.1.1. Introduction and classification

The term duplex stainless steel refers to Fe-Cr-Ni alloys where two phases (austenitic and ferritic) are present in considerable volume fractions (30% to 70%, but preferably 50%) in the microstructure. Due to its increased corrosion resistance and mechanical properties this stainless steel grade has applications in several sectors (1).

An empirical relationship between the chemical composition of the alloy and the corrosion resistance, called Pitting Resistance Equivalent (PRE) is used to categorize stainless steels (2):

$$PRE = \%Cr + 3.3 \times (\%Mo) \quad \text{Equation 1}$$

$$PRE_N = \%Cr + 3.3 \times (\%Mo) + 16 \times (\%Ni) \quad \text{Equation 2}$$

$$PRE_{NW} = \%Cr + 3.3 \times [\%Mo + (0.5 \times \%W)] + 16 \times (\%Ni) \quad \text{Equation 3}$$

Although, the Pitting Resistance Equivalent can take several forms due to its empirical nature, it is the most accepted and widely used method of categorizing alloys with respect to their corrosion resistance (1).

Table 1 contains the approximate chemical composition of different grades of super duplex stainless steels and their $PRE_N$ (2):

*Table 1. Typical chemical composition (in weight %) of stainless steels and their pitting resistance equivalent number. Adapted from (2).*

| *UNS* | *Cr* | *Mo* | *Ni* | *Mn* | *Cu* | *N* | *W* | *PRE* |
|---|---|---|---|---|---|---|---|---|
| *S32750* | 25 | 3.5 | 7 | 1 | 0 | 0.27 | 0 | 41 |
| *S32760* | 25 | 3.8 | 7 | 1 | 0.7 | 0.27 | 0.7 | 42 |
| *S32520* | 25 | 3.5 | 7 | 1 | 1.5 | 0.25 | 0 | 41 |

The super duplex term is applied to alloys with roughly 25%Cr, 3.5% Mo, and 0.2%N and $PRE_N$ value above 40. For comparison, the austenitic stainless steels UNS 304L and 316L have $PRE_N$ values of 18 and 24 respectively (2).

### 2.1.2. Microstructure and phase formation of Duplex Stainless Steels

To attain the duplex structure (Figure 1) the chemical composition of these alloys is engineered with elements that will favor austenite formation (Ni, C and Mn) and other elements that are ferrite stabilizers (Cr, Mo, Si, Nb). With Ni and Cr being the major contributors, two equations are used to calculate the Ni and Cr equivalents (2):

$$Ni_{eq} = [\%Ni + (30 \times \%C)] + (0.5 \times \%Mn) \quad \text{Equation 4}$$

$$Cr_{eq} = \%Cr + \%Mo + (1.5 \times \%Si) + (0.5 \times \%Nb) \quad \text{Equation 5}$$

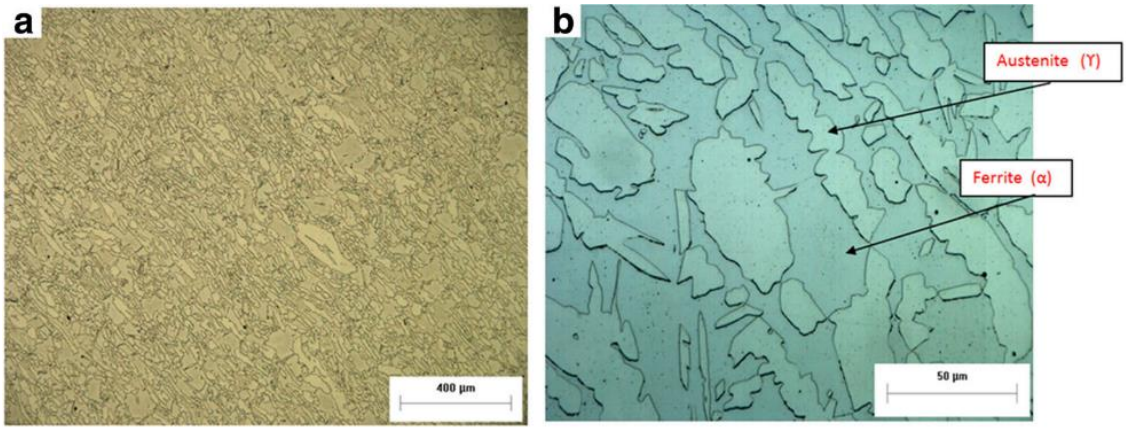


*Figure 1. SEM micrography of the duplex microstructure composed of the austenite (brighter) and ferrite (darker) phases. Used with permission (9).*

Duplex alloys are found in between the austenitic and ferritic regions, with ferrite content varying from 20 to 80% (10). When cast, duplex stainless-steel (DSS) first solidify as a ferritic alloy, and, at lower temperatures the austenite forms by a solid-state reaction. The ratio between austenite and ferrite is then preferably, but not always, kept at equal volumetric fractions by simultaneously controlling the chemical composition and cooling rate. The alloying elements present in the constitution of DSS, as well as heat treatment techniques, play an important role in their rather complicated precipitation behavior (11).

The number of possible coexisting phases in a microstructure depends directly on the number of alloying elements and heating/cooling conditions. Therefore, due to the presence of various chemical elements (Table 1), stainless steels are prone to intermetallic, carbide, and nitride phase formation. These secondary phases are, by their nature, hard and brittle, which can affect the mechanical properties of the bulk material (10,11). The major secondary phases observed in temperatures below 1000$^{o}$C are the sigma (σ), chi (χ),

carbides and nitrides, and finally the alpha-prime (α'). However other phases can also precipitate, such as the secondary austenite ($\gamma_2$), epsilon (ε), Laves (R), pi (π) and tal (τ) phases (1,2,10–12).

It is valuable to present, in a concise manner, the role of each alloying element in the microstructure of DSS (1):

| | |
|---|---|
| Chromium (Cr): | strongly affects the corrosion and oxidation resistance properties and is associated with ferrite, σ, χ, α', carbides and nitrides formation. In DSS a minimum of 20%Cr is required. |
| Molybdenum (Mo): | akin to Cr, Mo is a ferrite stabilizer, however, Mo has its own mechanism of increasing oxidation resistance properties. Its contribution to the $PRE_N$ is more than 3 times that of Cr. The χ, Laves and π phases are clearly influenced by Mo content since they are rich in this element. |
| Nickel (Ni): | is the major austenite stabilizer. Its content should be carefully controlled in order to obtain the desired duplex microstructure. In correct quantities, it slows down intermetallic phase formation in the austenitic matrix, but in excess it may accelerate the growth of secondary phases, mainly α' phase. Ni is closely related to oxidation resistance and mechanical properties due to its effect on the microstructure of stainless steels. |
| Nitrogen (N): | is crucial in duplex and super duplex stainless steels for numerous reasons. For instance, it increases $PRE_N$ by a factor of 16, |

contributes to austenite formation and strengthens the austenitic matrix by dissolution. N and Mo have a synergetic effect that enhances corrosion resistance properties even further. It allows the control of σ and χ precipitation and has the counterintuitive effect of reducing nitride formation.

Manganese (Mn): has no direct effect on phase balance. However, it is used to enhance the solubility of N. Mn may improve some properties, but in incorrect fractions, it aids in the precipitation of σ.

Copper (Cu): is austenite-stabilizer, reduces corrosion rate in acid environments and may improve the machinability of the alloy. Its presence can lead to precipitation hardening of Cu-rich ε precipitates.

Tungsten (W): improves pitting resistance and corrosion in chloride solutions although promotes intermetallic precipitation at elevated temperatures and secondary austenite ($\gamma_2$) formation after welding.

Silicon (Si): enhances corrosion and oxidation resistance properties and promotes σ and G-phase precipitation.

Carbon (C): has its content generally restricted to 0.02% or 0.04% to prevent carbide precipitation, in most wrought DSS.

Sulphur (S) is defined and controlled by steel making processes. S may be beneficial for welding or machining.

### 2.1.3. Properties of Duplex Stainless Steels

This part of the literature review will address some of the mechanical and physical properties of DSS and SDSS.

#### 2.1.3.1. Mechanical Properties

The duplex microstructure combines the high plasticity of ferrite phase and austenite's increased yield strength. DSS and SDSS alloys have high strength with good toughness and ductility. Several mechanisms are connected to their mechanical properties (1,10).

- Interstitial solid solution hardening by C and N.
- Substitutional solid solution hardening due to the solubilization of metallic elements.
- Grain refinement strengthening, caused by the existence of two phases.
- Precipitation hardening caused by secondary phases.

Regarding tensile properties (Table 2), duplex alloys have superior yield ($R_{p0.2}$) and ultimate ($R_m$) strengths when compared to ferritic and austenitic stainless steels. S32750 shows very high strength although the elongation at fracture ($A_5$) is as low as ferritic alloys (1,10,12,13).

*Table 2. Mechanical properties of some ferritic, austenitic, and duplex stainless steel alloys. Adapted from (1).*

| | *Grades* | *$R_{p0.2}$ (MPa)* | *$R_m$ (MPa)* | *$A_5$ (%)* | *Hardness (HB)* |
|---|---|---|---|---|---|
| *Ferritic* | S40900 | 205 | 380 | 20 | 179 |
| | S44700 | 415 | 550 | 20 | 223 |
| *Austenitic* | S31603 | 170 | 485 | 40 | 217 |
| | S31254 | 300 | 650 | 35 | 223 |
| *Duplex/ Super Duplex* | S31200 | 450 | 690 | 25 | 293 |
| | S32550 | 550 | 760 | 15 | 302 |
| | S32750 | 550 | 795 | 15 | 310 |

Figure 2 illustrates the yield strength of different duplex stainless steels as a function of temperature. Most duplex stainless steels retain a good portion of yield strength up to 300°C. The alloy S32750 (2507 in the graph) outperforms S32760 in this matter, preserving more strength at elevated temperatures. In comparison to the 316L austenitic alloy, it is roughly three times stronger at 300°C (1,12).

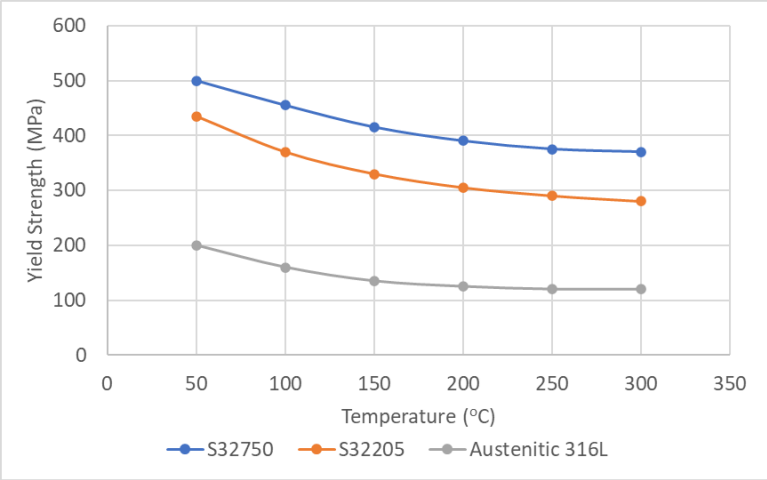


*Figure 2. Temperature influence on different grades DSS and the 316L austenitic stainless steel. Based on* (12).

Cold working can lead to work hardening and is therefore important evidence of the DSS behavior under plastic deformation. As depicted in Figure 3, cold working leads to a sharp increase in mechanical properties followed by loss of ductility (12).

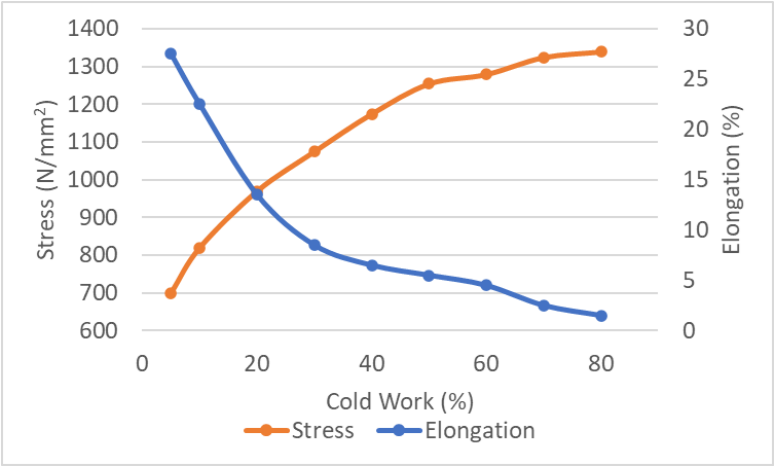


*Figure 3. The change in the mechanical properties of cold-worked 2205 duplex stainless steel. Based on* (12).

#### 2.1.3.2. Physical Properties of DSS

In general, the physical properties of DSS are comparable to austenitic stainless steels (Table 3). The specific heat falls in between austenitic and ferritic stainless steel. The adverse implications on the machining performance of DSS due to its low thermal conductivity could be severe. If the heat in the cutting zone does not properly propagate, it may favor the localized embrittlement of the alloy due to the formation of secondary phases that increase the hardness of that respective region (1,14).

*Table 3. Thermal properties of some stainless steels. Adapted from* (1,14).

| *Type* | *UNS* | *Thermal Expansion Coefficient ($10^{-6}$ $K^{-1}$)* | *Specific Heat Capacity ($J.kg^{-1}K^{-1}$)* | *Thermal Conductivity ($Wm^{-1}K^{-1}$)* |
|---|---|---|---|---|
| *Ferritic* | A516 | 12.5 | 450 | 60 |
| | S44700 | 10 | 480 | 21 |
| *Austenitic* | S30400 | 16 | 520 | 16 |
| | N08904 | 16 | 544 | 15 |
| *Duplex* | S31803 | - | 470 | 14 |
| | S32304 | 13 | 470 | 16 |
| *Super Duplex* | S32750 | 13 | 470 | 14 |
| | S32760 | 12.8 | 482 | 12.9 |
| | S32520 | 13.5 | 450 | 17 |

## 2.2.Machining

### 2.2.1. General aspects of machining and metal cutting

Machining is a very versatile manufacturing process that is capable of being applied as a primary or secondary operation to obtain high-quality surfaces with very high dimensional accuracy. Metallic and non-metallic (polymers, ceramics, and wood)

workpieces can be processed through machining (15–20). This literature review will focus on metal cutting by turning operations since it is the most pertinent topic to the research.

### 2.2.2. Cutting Forces

As the cutting tool approaches the workpiece to perform the cut, it exerts a force that can be measured through three components ($F_c$, $F_t$, $F_r$)(15,19,20).

$F_c$: The cutting force that acts in the direction of the cut (along the y axis).

$F_t$: The thrust force that acts in the feed direction (along the x axis).

$F_r$: The force that pushes the tool away from the workpiece (along the z axis). Usually disregarded due to a much lower value compared to the other two components.

These force components are strongly affected mainly by workpiece and cutting tool material properties and geometry, as well as, clamping, cutting parameters (depth, speed, feed), and cooling/lubrication (15,18–20). It is not possible to directly measure these forces, however, a specifically designed dynamometer can measure the deflection or strain that is induced in its structure and correlate them to $F_c$, $F_t$, and $F_r$ (16,18).

The knowledge of the cutting forces, that are generated during metal cutting, can be used as a powerful tool for research and manufacturing machining projects for several reasons (15,16,18,20):

- It is a major indicator of the machinability of materials.

- It allows for the design/selection of appropriate workpiece materials, cutting tools (material and geometry), cutting parameters (depth, speed, feed), cutting fluid/coatings, machine tool elements, tool holders and fixtures, etc.
- The amount of power consumed is directly related to the cutting forces. By calculating the power requirement, it is possible to optimize production costs and choose the most suitable electric motor for a determined operation.
- The force acts on the workpiece and causes deflection of the workpiece, tool or machine leading to the inaccuracy of the machined surface, high temperature generation, and unstable vibrations.
- Tool wear and failure can be monitored.

### 2.2.3. Cutting Temperature

Virtually, all the mechanical energy applied through the cutting speed is converted into thermal energy due to friction between the tool and workpiece, but also because of the formation of the chip. As the cutting area can be divided into three shear deformation zones, temperature affects them differently (15,16,19–21):

*PSDZ:* The temperature increase in the chip-formation zone directly affects the mechanical properties of the workpiece and, consequently, the cutting forces.

*SSDZ* In the secondary shear deformation zone, high temperature can accelerate oxidation and diffusion and also soften the cutting

tool making it more susceptible to wear. Since tool life is generally an important requirement, the temperature on the rake face of the tool can restrict the maximum cutting speed in many applications.

TSDZ The temperature in the clearance face of the tool impacts the surface integrity of the machined part by inducing residual stresses, due to thermal contraction, or even by creating a hardening layer.

The process parameters (speed, feed rate and depth of cut) are variables that affect heat generation during cutting. Speed being the major influence. However, the workpiece material properties, as well as the angle and geometry of the tool also play an important role in cutting temperatures (15,16,19–21). Figure 4 shows the changes in temperature during the cutting of S32750 SDSS at different cutting speeds. The temperature drastically increases from varying the cutting speed from 60 m/min to 120 m/min under dry conditions. The application of a coolant reduces the cutting temperature in about 60% at higher cutting speeds (22). Since S32750 SDSS contains many elements in its chemical composition, it is possible that hard and brittle phases such as sigma (σ) or chi(χ) form during cutting, thus negatively impacting the cutting operation (22). Temperature-induced problems can greatly influence any machining process by decreasing final product quality and creating delays due to machine downtime. Therefore, from a manufacturer's point of view, it makes sense to control the temperature within the cutting zone and keep it as low as possible.

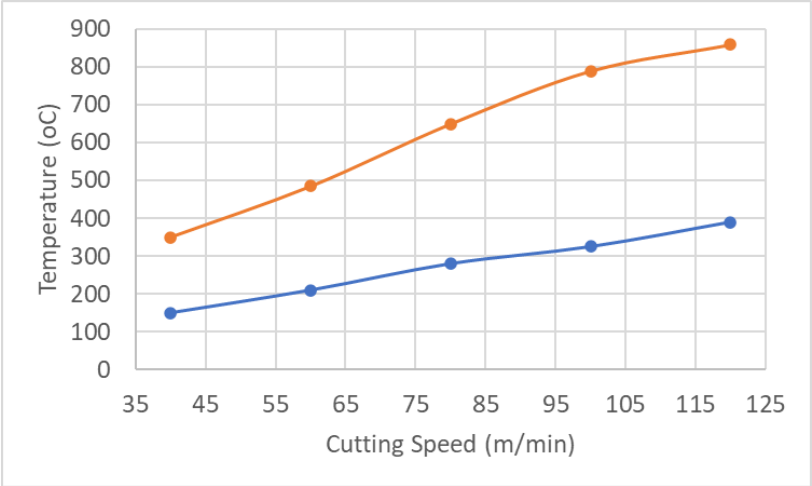


*Figure 4. The change in temperature at different cutting speeds with constant feed rate and depth of cut when machining S32750 SDSS. Based on* (22).

### 2.2.4. Chip Formation

The process of metal removal starts when the shear force imposed by the cutting tool overcomes the yield strength of the workpiece material which, then, deforms plastically forming the chip. This happens in the primary shear deformation zone (Figure 5). Describing the chip formation is a complex task because it involves several different mechanisms that depend on the workpiece and tool materials, as well as the cutting parameters and conditions. Therefore, some simplifications must be applied for a general understanding of the events that take place in metal cutting. It is agreed by many authors that as the cutting continues, two zones are formed at the tool/chip interface (15,16,18–20).

- A sticking zone: the tool edge, where the workpiece material gets attached to the tool tip due to the interaction, at the atomic level, between both the tool and the workpiece materials.

- A sliding zone: within which the chip slides on the rake face of the tool until it leaves the system.

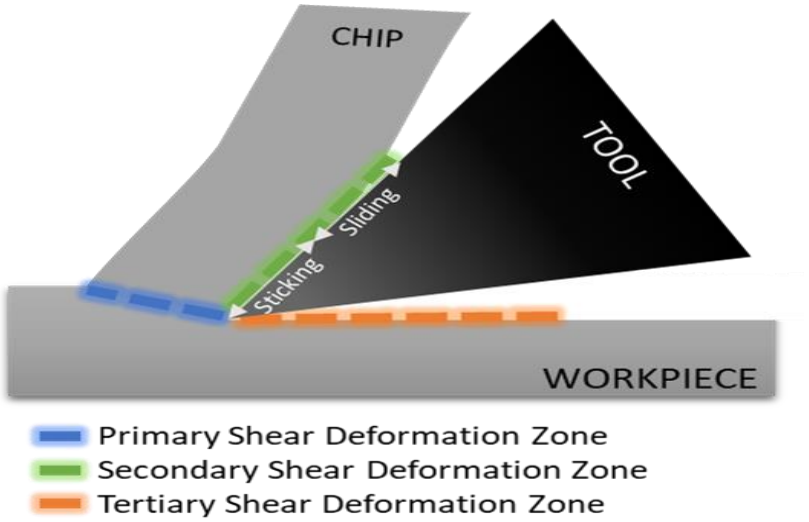


*Figure 5. A representation of the chip formation and the shear deformation zones. Based on* (7).

Generally, when cutting hard and brittle materials, the strain and stress within these zones can fracture the material leading to discontinuous chip formation. For example, when machining gray cast iron (Figure 6 – a). Ductile materials, on the other hand, produce continuous chip segments, which can absorb more energy without fracturing (Figure 6 – b). The bonding withing the sticking zone may, under some circumstances, give birth to a built-up edge (BUE) where workpiece material adheres to the edge of the tool changing its shape (Figure 6 – c). Another type of continuous chip happens if the chip does not fracture but still undergoes localized heavy plastic deformation, for example, when the mechanical properties of the material change with temperature. This results in a shear-localized chip

with a serrated morphology where narrow heavily deformed bands of material alternate with wider bands of undeformed material (Figure 6 – d) (16,23). These four basic types of chips are illustrated below:

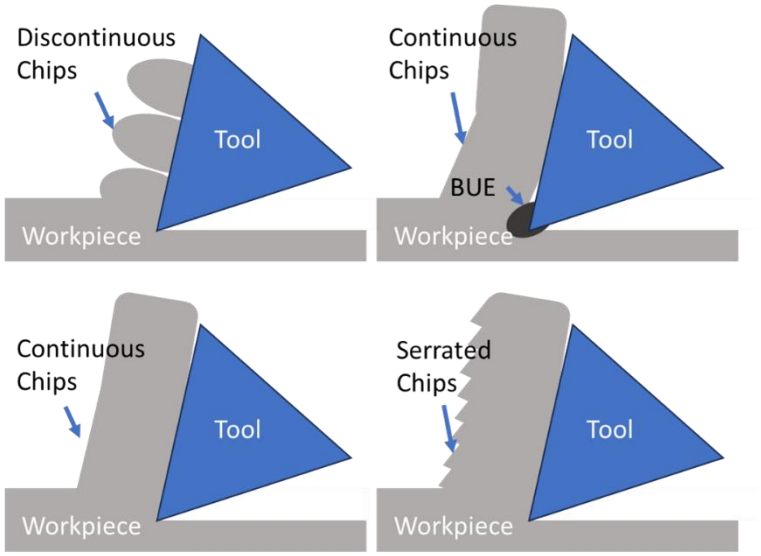


*Figure 6. Types of chip formation. Based on* (16).

The chip carries important information regarding the cutting events and is extensively used not only for research purposes but also in manufacturing. Characteristics like morphology, microstructure, composition, cross-section thickness, undersurface topography, and shear-angle can be linked to the behavior of the workpiece material in response to the machining operation (15,16,18–20).

The characterization of S32750 SDSS chips obtained at different cutting speeds can be seen in Figure 7. The topographic analysis revealed that the undersurface of the chip produced at lower cutting speed was rougher. Although the difference was not very

significant, it indicates slightly more severe frictional conditions in the tool/chip interface at lower speeds (5).

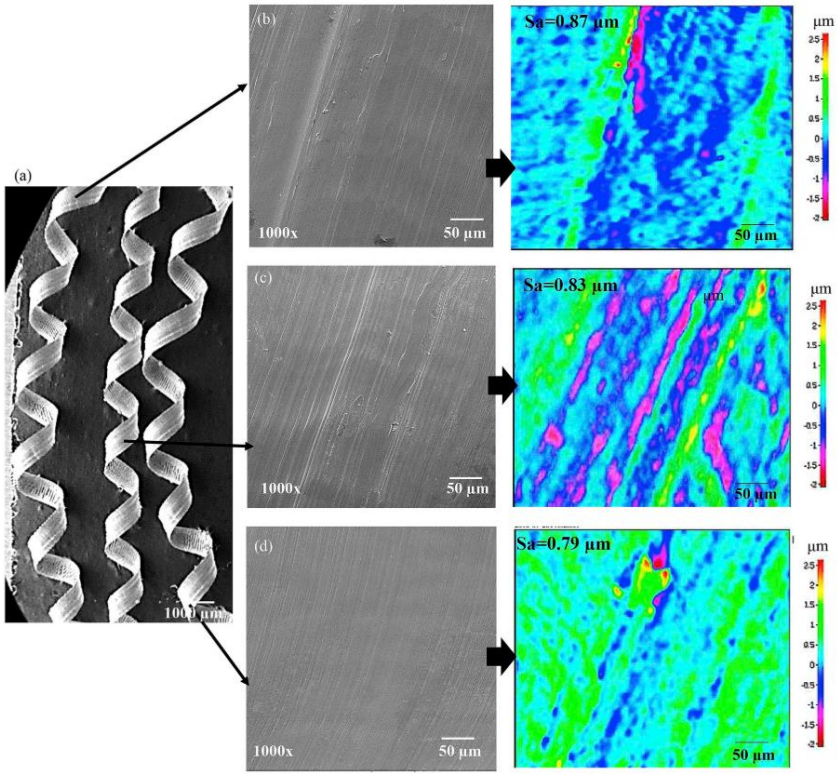


*Figure 7. The undersurface roughness of three different chips of S32750 machined at 60 m/min (b) 100 m/min (c) 150 m/min (d). Used with permission (5).*

Additionally, Figure 8. shows that turning S32750 SDSS produces serrated chips. The micrograph also provides a measurement of maximum and minimum chip thicknesses and shear angle of chips that were cut at 150 m/min. This data can be used to investigate the friction conditions withing the chip/tool interface. The serrations on the chip morphology happen due to shear stress localization that is a characteristic of materials that are difficult to cut (5).

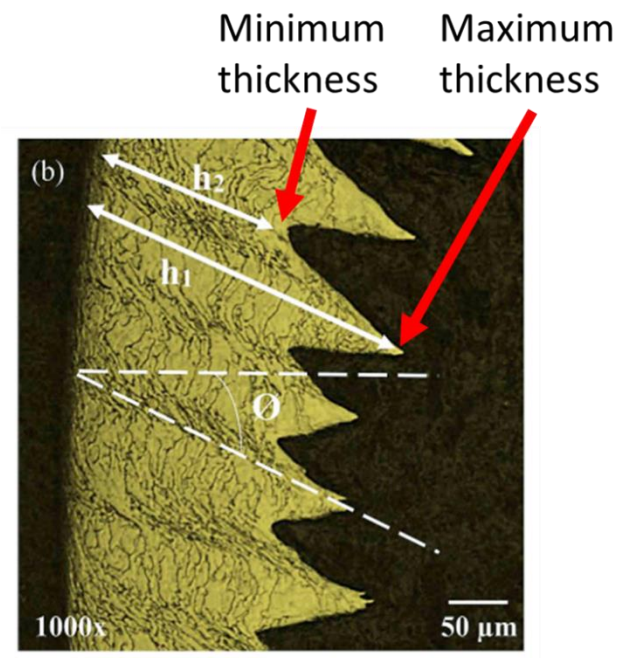


*Figure 8. The chip microstructure of S32750 machined at 150 m/min with. Used with permission (5).*

With specific devices, such as the quick-stop device, it is possible to immediately stop the cutting process leaving the chip still attached to the workpiece. This quick-stop specimen can be further examined in order to better understand the chip formation mechanism. Figure 9 is a representation of Knoop microhardness measurements that were carried out in quick-stop samples of S32750 based on data from (24). It is possible to see that S32750 SDSS is susceptible to work hardening effects during machining. Also, the layer that slides on the rake face of the tool (secondary shear zone) is much harder than the original material, this intensifies frictional events and accelerates tool wear on that region.

The primary shear deformation zone is also hardened, which also affects wear and cutting forces (24).

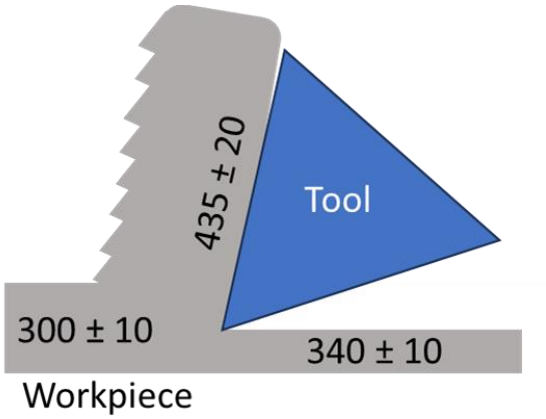


*Figure 9. Knoop microhardness measurements on S32750 quick-stop specimens. Based on* (24).

### 2.2.5. Built-up Edge Formation

The microstructural and mechanical properties of S32750 favor the formation of the built-up edge when this stainless steel grade is being cut. BUE, as previously mentioned, happens when workpiece material sticks to the cutting tool edge. This material suffers extremely high compressive stresses capable of heavily deforming its microstructure, to the point that the yield strength rises so much that the shear stress applied by the tool cannot break the bond between the cutting edge and the BUE. Layer upon layer the material adhering to the work tool gradually increases the BUE size and yield strength. At any point in time, the shear stress exceeds the yield strength of that work hardened region, the BUE becomes unstable, snaps off and is carried away with the chip. Soon after, a new BUE will

start forming again and this cyclic process is repeated. Whenever the BUE breaks off, it may be so strongly bonded to the cutting tool that, it can remove material from the edge, causing adhesion wear and decreasing tool life (5,15–17,19,20,24,25).

With the exception of specific cases, where the BUE acts as a protective layer, it is usually treated as an undesirable side effect of machining ductile materials at low cutting speeds, because it drastically affects the surface integrity, cutting forces, effective feed rate, rake angle and tool wear. There are some available alternatives to reduce or eliminate the negative effects associated with BUE formation. The first and easiest way would be to increase the cutting speed, however, this is not always possible. In these cases, it is feasible to reduce the work hardening effect, that causes BUE to form, by applying lubricants or changing the tool surface by coating technologies (5,15–17,19,20,24,25).

### 2.2.6. Surface Integrity

One of the main goals of using machining as a processing method is to produce surfaces with consistent dimensions, forms, and finishes for a wide range of applications. Due to quality and functional requirements, surface integrity can be a limiting factor when choosing the appropriate tool and selecting the best cutting parameters. In manufacturing, the surface finish comprises a great share of production costs and is, therefore, reflected back in the final price of the product (15,16,19,21).

Profilometers, 3D microscopes and other specific devices can measure the surface roughness by calculating the mean deviation of the height between the peaks and valleys present in the surface of the material (Ra). In other words, high Ra values correspond to

rougher surfaces. The microhardness profile testing also provides good information on the mechanical properties of the surface and on the behavior of the material during cutting. The surface hardness tends to increase due to work hardening effects and, sometimes, due to the precipitation of secondary phases in the microstructure. By examining the surface with respect to its hardness distribution it is possible to adjust input variables, thus improving machining operations (15,16,19,21)

### 2.2.7. Machinability

Quantifying machinability is far from a trivial task because it does not correspond to an absolute property of materials. Many possible interpretations can be made to suit specific requirements. Generally, it is accepted that when a material has good machinability, it may be processed with reduced power consumption, extended tool life and, at the same time, promoting an acceptable surface finish. It is a very specific property that depends not only on the material but also on several other factors, such as (3,15,16,18–20):

- Workpiece physical and mechanical properties
- Tool geometry and material
- Type of operation (roughing or finishing)
- Machine characteristics (power, rigidity, and accuracy)
- Machining conditions and environment (coolant cycles, parameters, etc.)
- Chip formation
- Frictional conditions and built-up edge

It is generally accepted that the machinability criterion should be adopted relative to the type of operation. When roughing, tool life and power consumption are more important factors than surface finish. Whereas the latter is the major concern when it comes to finishing. Therefore, a material might be machinable under certain conditions but not equally suitable for machining if these conditions are altered. This is the reason why machinability is evaluated for each specific case (3,15,16,18–20).

For the reasons previously stated, machinability has no unit and is rather evaluated by comparison between different materials. Stainless steels are considered either poor or very poor in terms of machinability, special attention should be given to duplex and super duplex alloys since they are as hard to machine as high speed steels (HSS), a material commonly used for cutting tool production (3).

The diagram in Figure 10 summarizes the aspects involved in assessing the machinability of materials, including the input and output variables that were previously mentioned.

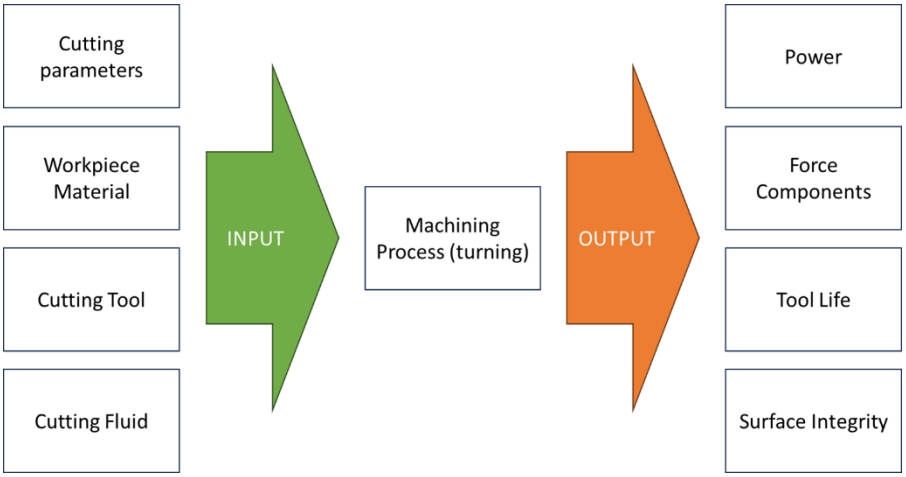


*Figure 10. The input parameters and output variables that affect the machinability criteria. Based on (3).*

Super duplex stainless steels are more challenging to machine than austenitic grades. The determining factors for the machinability of these alloys are the increased number and content of alloying elements (especially Cr, N and Mo), the duplex microstructure and the overall mechanical and physical properties (3).

## 2.3. Cutting Tools

The constant need to increase production output added to the demand for machining new materials acted as the two major driving forces for the continuous development of cutting tools (3,15,16,19,20).

Designing new/enhanced cutting tools has the ultimate goal of increasing machining performance and reducing the negative effects of tool wear mechanisms while providing consistent surface finish. The tools are exposed to severe conditions throughout the cutting process, for example intense friction and stress. In some circumstances,

temperatures can reach up to 1000ºC in the cutting zone, which accelerates tool wear mechanisms. There is no ideal tool that can withstand all types of cutting conditions and, therefore, effectively machine the extensive list of materials demanded by industry. Such ideal tool would require the following properties (3,15,16,19,20):

- High hardness at elevated working temperatures.
- High strength and toughness.
- High fatigue strength.
- High wear resistance.
- Inertness and chemical stability.
- Thermal shock resistance.
- High thermal conductivity.
- Low coefficient of friction.
- Low cost and high availability.

A material that has all the previously mentioned characteristics is yet to be discovered. In reality, the balance between these properties will determine the most suitable application for each type of tool material. Choosing the correct tool material is critical to most machining processes. Some cutting tools have excellent properties, however, they have limited applications, for example, due to chemical incompatibility with the workpiece material (3,15,16,19,20).

### 2.3.1. Cutting tool materials

Carbon tool steel (CTS) prevailed as the only material used for the fabrication of cutting tools for years. Over this period, the carbon content was optimized, and heat treatments were created to tackle particular cutting operations. While carbon steel tools made it possible to cut copper at relatively high speeds (about 110 m/min), their performance for cutting iron and other steels was not even close to that (5 m/min). This low production speed was enough to cope with the demands imposed by manufacturers leading to the development of new tool materials such as high speed steels (HSS), cast nonferrous alloys (Stellite and UCON), cemented carbides (Widia and TiC-based), cermets, ceramics, SiAlON, cubic boron nitride (CBN) and diamond (PCD)(3,15,19).

### 2.3.2. Tool wear

Tool failure occurs in response to wear, plastic deformation, or fracture. Several mechanisms are involved in tool wear. Tools may deform plastically or even fracture when they are incapable of withstanding the loads generated during the cut. The study of tool wear is crucial because of the strong relationship between tool life, production costs, and quality. Good industrial practices tend to eliminate unnecessary costs related to replacing tools as much as possible. Ideally, tools should wear slowly so that dimensions and surface finish are kept consistent for a prolonged time (16,20).

With respect to wear, two regions on the tool surface are of interest, the relief (or clearance) and the rake faces. The former is mainly affected by flank wear, while crater wear occurs on the rake face. Flank wear produces a wear land that can be measured by its

average or maximum width. At the beginning of the tool life, the rate of flank wear is accelerated, when the cutting edge is rounding, then, the flank wear progression should steadily proceed at a slower rate until the critical land width is reached. At this point, the surface integrity is strongly impaired, and the tool becomes unusable. Crater wear is characterized by the depth of the crater that forms on the rake face. It can weaken the cutting edge and ultimately lead to tool fracture (16,20).

There are other types of wear, such as notch wear that happens due to the interaction of the tool with the formed chips when machining hard materials, nose radius wear which also impacts surface finish, thermal and mechanical cracking that result from cyclic loads and high tool/chip interface temperatures, edge chipping when using brittle tool materials, and chip hammering can occur when the chip curls back and hits the tool face. Figure 11 illustrates these different types of wear (16,20).

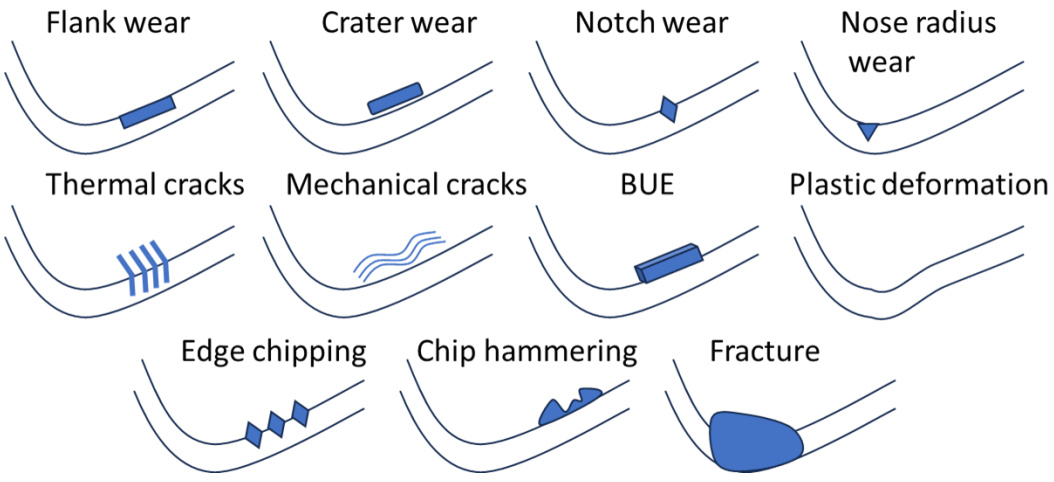


*Figure 11. Different types of cutting tool wear. Based on* (16).

Machining super duplex stainless steels involves high heat generation, surface work hardening, and formation of BUE which intensify wear mechanisms such as adhesion, oxidation and, ultimately, chipping of the cutting tool (3,4). As an example, Figure 12 contains amplified images of the tip of carbide inserts after turning S32750.

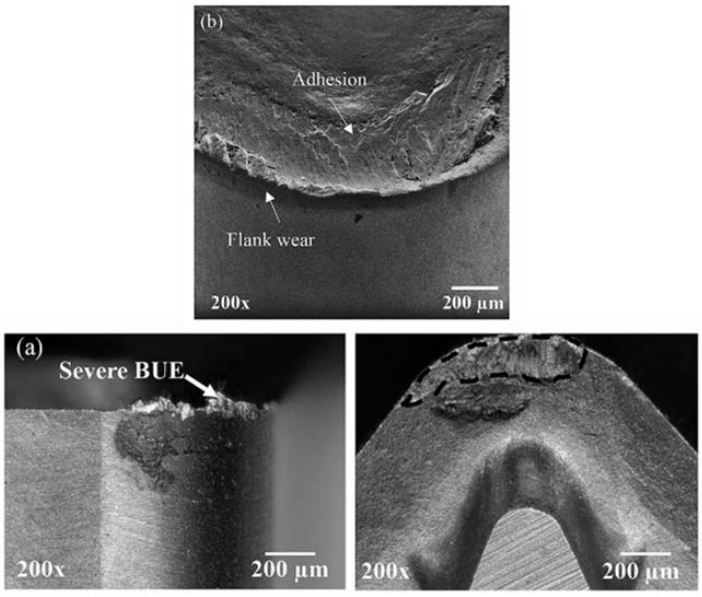


*Figure 12. Example of tool wear after turning S32750. Used with permission (5).*

### 2.3.3. Tool wear mechanisms

It is important to note that the frictional events that take place between the tool, workpiece and chips involve high temperature and pressure, as well as the creation of a new surface that has a strong tendency of bonding. The consequences are the different tool wear mechanisms (16,20):

| | |
|---|---|
| Adhesive wear | Tool material adheres or welds to the chip and is carried away leaving a crater on the rake face of the tool. It is accelerated by BUE formation and low cutting speeds. It can cause tool chipping. |
| Abrasive wear | Hard abrasive particles remove material from the flank face of the tool. It is usually associated with flank, notch, and radius wear. Therefore, it is crucial to monitor and prevent this type of wear. Especially at low to medium cutting speeds. |
| Diffusion wear | Tool material from the rake face dissolves into the chip weakening the surface and leading to crater wear. The solubility of the tool material in the workpiece, the contact time and the temperature at the tool/chip interface influence the rate of this type of wear. |
| Oxidation | The reaction between oxygen in the atmosphere and the tool constituents at high temperatures results in severe notch wear. |
| Corrosion | When highly reactive materials are machined, chemical reactions between the tool, the workpiece or even the cutting fluid can take place, causing flank and crater wear. |

## 2.4. Surface Engineering and Coated Cutting Tools

The surface of a solid is defined by the region that interacts with the environment. The ideal surface would be the very last layers of atoms present in the solid, however in reality, the surface extends to the region where the properties (mechanical, microstructural and physicochemical) drastically differ from the bulk. The real surface may comprise several different zones or layers. A first layer corresponds to the adsorbed gases that are present in the atmosphere, right below this first layer, a second oxide/nitride/carbide layer

is formed by the chemical reaction between the very last atomic layer of the solid with O, N and C also present in the atmosphere. A third and fourth layers are formed as a consequence of the work hardening imposed by the processing conditions of the solid, the third layer is severely affected by mechanical strain and, therefore, has no crystallinity. Whereas, the fourth and usually larger layer, has its crystal structure deformed by the accumulation of residual stresses (26–28).

The surface is the boundary between the bulk material and the environment and, therefore, is submitted to several phenomena, for example, wear, fatigue and corrosion. As a consequence of these phenomena, most failures occur on the surface. The bulk or core material must be able to withstand the loads imposed by the application, while the surface is responsible for interacting with the external conditions to which the material is submitted (26–28).

By engineering the surface of materials, it is possible to enhance specific properties and, thus, improve their response to said phenomena. This can be accomplished by an overlay process, a surface modification process or even different combinations of both (26,27):

Overlay process: The substrate surface is covered by a layer of the deposited material. For example, coating and thin-film deposition.

| | |
|---|---|
| Surface modification: | The substrate surface is modified, yet the material remains the same. For example, plasma nitriding, aluminum anodization, etc. |

These processes can be used interchangeably, meaning that the surface of the substrate can be modified prior to a coating deposition or even the surface of the coating itself can have its properties altered. The deposition of a new material layer can be done atomistically (atom-by-atom) and produce a wide variety of films that differ in terms of crystal structure, density, purity and thickness. Thin film is the term commonly applied to layers no more than a micron thick. Whereas coatings can be slightly thicker (26,27).

### 2.4.1. Types of coatings for cutting tools

Coatings can be deposited via several different methods which can be conveniently divided into four groups that are classified with respect to the state of the depositing phase (gaseous, solution, molten, semi-molten and solid-state processes). The two major techniques that are used for cutting tools are gaseous state processes known as chemical vapor deposition (CVD) and physical vapor deposition (PVD). In CVD, a thermochemical process, gaseous chemical reagents are used as the source of coating material, while the latter, a physical process, consists of the evaporation/atomization of the coating material from a solid kept in the coating chamber. CVD processes are capable of producing thick coatings, which are often times preferable for roughing operations, as opposed to thin PVD coatings that are good for finishing (6,26).

### 2.4.2. PVD processes

PVD processes are atomistic processes where atoms in the vapor state are deposited onto the substrate via condensation. A few to a thousand nanometers in coating thickness can be achieved, in addition to multilayered architectures with these processes. PVD offers versatility in terms of substrate size and shape. It is possible to produce coatings of pure elements, alloys and compounds. Compound coatings can be deposited by reactive processes where the depositing material and a gas such as N or a co-depositing material (carbon) react to form carbides and nitrides on the surface of the substrate (6,26).

The PVD processes can be grouped into 4 general categories (6,26):

- Vacuum Evaporation: carried out in vacuum ($10^{-5}$ to $10^{-9}$ Torr) to reduce contamination. Higher vaporization rates are achieved by thermally heated sources (wire coils or electron beam). Used for optical interference coatings, mirror coatings, decorative coatings, permeation barrier films, electrically conducting films, wear resistant coatings, and corrosion protective coatings.

- Sputtering: Non-thermal vaporization processes where the sputtering source (element, alloy, mixture or compound) is bombarded by ions that transfer momentum energy and physically remove the surface atoms in the form of vapor with the bulk composition of the target. Different sputtering configurations are available (ion beam, magnetron, high power impulse magnetron - HiPIMS, rf

sputtering, etc.). Used in semi-conductors, architectural glass, CDs, magnetic films, dry film lubricants, hard and decorative coatings.

- Arc vapor deposition: A high current and low voltage arc is used to vaporize an electrode (anodic or cathodic) made of the source material (element, alloy, mixture or compound precursor) producing a highly ionized vapor that is accelerated towards the substrate surface. Used for hard and decorative coatings.

- Ion plating: Uses the energy, flux and mass of energetic particles (ions) and the vaporized material (bombarding species extracted either from evaporation, sputtering, arc or a chemical precursor) to modify and control the properties of the depositing coating. The ions can be extracted from plasma or by an ion gun. Used for hard coatings, metal coatings, high-density optical coatings.

The properties of PVD coatings are strongly affected by the substrate surface condition (roughness, contamination, chemistry, mechanical properties, geometry, preferential nucleation sites, stability), the deposition process variables (type, substrate temperature, deposition rate, angle of incidence, contamination, ion plating), the particularities of film growth (condensation, nucleation, interface formation, morphology of the film, changes in film properties during deposition), intermediate processing (periodic ion bombardment, oxidation, wiping or burnishing between layers) and post-deposition processing (reaction

between the film and the environment, thermal or mechanical cycling, corrosion, shot peening, chemical modification) (6,26).

Therefore, the mass production of PVD coatings with consistent properties depends on various factors that must be reproducible. For example, the real surface of the substrate, contaminants, cleaning, other sources (film material build up on fixtures and chamber, degradation of the vacuum system, etc.). There is a vast range of PVD processes to cover the most varied demands imposed by industry (6,26).

### 2.4.3. Arc vapor deposition

An electrode (cathode or anode) is vaporized by a high-current, low-voltage electrical arc. Most of the vaporized target material is atomized, however molten droplets or even solid particles from the electrode can be ejected in the process as well. The vapor is allowed to condense on the substrate, forming the film layer.

The arc vapor deposition may be carried out in vacuum or even in low pressure gaseous environments (6,26):

*Vacuum Arc*

In a high vacuum ($10^{-5}$ Torr), the arc is initiated by firstly touching the electrodes and then separating them by a small distance. The arc forms a highly ionized vapor that is accelerated towards the substrate at a high energy level.

*Gaseous Arcs*

For film deposition the gas pressure should be adjusted to a maximum of $10^{-2}$ Torr. Atoms from both the gas and the electrodes are ionized, allowing for a wider space between the electrodes. Inert and/or reactive gases can be used to form compound materials.

The vaporization can be achieved from either the cathode (cathodic arc) or anode (anodic arc) (6,26):

*Cathodic Arcs*

The cathode is molten. This process involves much higher electrical current densities, which results in problems with movement and stabilization of the arc and the formation of macros (globules of the ejected material).

*Anodic Arcs*

In processes where the anode melts the electrical current density is much lower. Therefore, the level of ionization of the vaporized anode material is less in comparison to cathodic arcs, but molten globules cease to be a problem.

### 2.4.4. Sputtering

Basically, the sputtering process consists of bombarding the target plate with energetic ions that are generated from the plasma. The number of bombarding atoms, therefore, is proportional to the rate of sputtered material. In basic sputtering processes, where the plasma is not properly confined, the deposition rates are low. The development of the magnetron sputtering allowed the mass production of dense high-quality films at low temperature by using a magnetic field to constrain the plasma to a region very close to the

target surface, which increases the ionization efficiency, the bombardment rate and ultimately, the deposition rate. Many different methods of operating the magnetrons can be used, for example (6,26,29):

*DC magnetron*

Used mainly for conducting targets. Although it is possible to deposit non-conductive materials such as $Al_2O_3$ in reactive deposition environments.

*AC and RF magnetron*

The potential on the target can be periodically reversed at different frequency ranges. Frequencies below 50 Hz characterize the AC magnetron sputtering, while RF (radio frequency) sputtering can apply frequencies in the range of 0.5-30 MHz. The latter is capable of sputtering electrically insulating materials at very low rates.

*Pulsed power magnetron*

Unipolar or bipolar square waveform pulses are applied on the target material at frequencies from 50 to 250 kHz. The pulsed power output can be controlled in terms of frequency, duration and voltage. In high power impulse magnetron sputtering (HiPIMS) the pulses are adjusted to very high peak voltage and power and applied in a very short duration. Thus, a high ionization of the vaporized material is achieved, increasing the plasma density. HiPIMS films have a dense microstructure, excellent adhesion, high corrosion, and wear protection capabilities (low coefficient of friction).

### 2.4.5. Tribological Properties

Cutting tools can have their tribological properties improved by surface engineering. Tribology, from the Greek word *"tribos"*, that means *"rubbing"*, is the science that investigates the interaction between two surfaces that are in relative motion and phenomena related to wear, friction, lubrication, corrosion and adhesion. During machining, the performance of cutting tools is heavily dependent on the tribological conditions to which their surface is subjected to. The properties related to wear resistance (namely hardness, chemical and corrosion inertness and coefficient of friction) of cutting tools may be significantly changed by the deposition of tribological coatings on their surface. Tribological coatings are designed to address conditions otherwise detrimental to the substrate material and are defined by a combination of properties such as hardness, elasticity, strength, toughness, thermal expansion, roughness and adhesion (6,27,28,30,31).

*Hardness*

The notion of how hard a material is depends on several different contributions from other basic properties such as yield strength, elastic modulus, true tensile strength, work hardening, etc. Nevertheless, hardness can be broadly described as the resistance to plastic deformation by indentation. When it comes to the workpiece, hard materials (such as super duplex stainless steels) have poor machinability and, therefore, cutting tools undergo intensive abrasive wear. In addition, hardness also serves as a valuable indicator of wear resistance when selecting cutting tools for machining these materials. Surface modification

and/or the addition of a coating layer can potentially increase the hardness of the surface of cutting tools, providing additional wear resistance (26,27).

Several methods can be used for measuring hardness. However, each method has its own peculiarities and thus, the magnitude of this property is linked to the type of test that was employed. Consequently, the same test should be carried out for hardness comparison purposes. Usually, micro and nanoindenters are used to assess the hardness of thin-films and coatings due to their microscopic dimensions (26,27).

The difference in hardness between the substrate (cemented carbide WC/Co) and three different coatings can be seen in Figure 13. The multilayer $Al_{50}Cr_{50}N + Ti_{95}Si_5N$ has almost two times the hardness of the substrate (9).

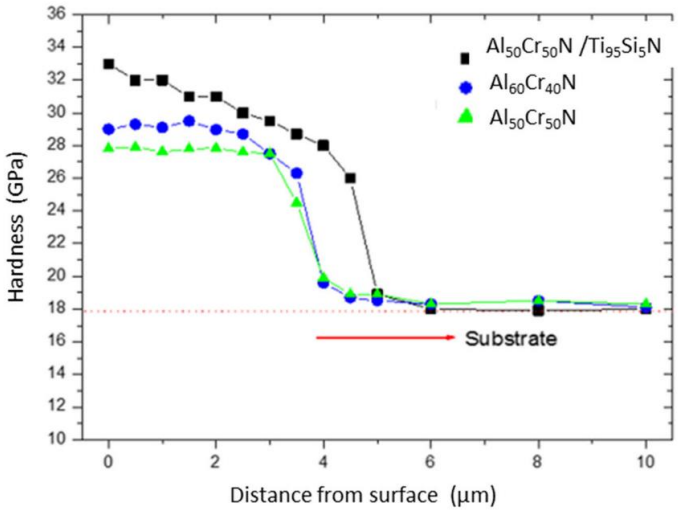


*Figure 13. Hardness profiles of three different coatings and the cemented WC/Co tool substrate. Used with permission* (9).

*Elastic strain limit and the plastic resistance parameter*

The coating's elastic strain limit can be calculated by the H/E ratio, where H and E correspond to the hardness and the elastic modulus, respectively. This ratio is proportional to the amount of energy the coating can absorb before permanent deformation takes place. Another variation of this ratio $H^3/E^2$, called plastic resistance parameter, can be calculated to assess the resistance to plastic flow of the coating. These ratios can be related to the plasticity index (PI), which corresponds to the capacity of the coating to dissipate frictional energy providing important information when selecting/designing coatings to ensure improved tool life. (6,32).

*Coefficient of friction*

When two surfaces are in relative motion, the resistance to that particular motion defines the phenomenon of friction. In a similar fashion to hardness, the coefficient of friction (COF) is a function of several material properties (surface roughness, as well as, mechanical and thermal properties), environmental conditions (temperature, humidity, lubrication), not to mention, the measurement method. Thus, COF depends on complex mechanical, physical and chemical surface interactions. The knowledge of the frictional conditions between the tool and workpiece allows for a better tool and coating selection, thus improving the machining process as a whole (better surface integrity and dimensional accuracy, reduced vibrations and tool wear and lower cutting temperatures) (26,27,32). Surface engineering provides solutions to reduce the coefficient of friction of the tool either by surface modification or coating deposition (7–9,26,27,32–35).

From Figure 14, it is possible to observe that uncoated tools endure more wear than coated ones in this application. Extended tool life was observed using the PVD AlTiN coating with a lower coefficient of friction, 0.267 compared to 0.404 of multilayer CVD TiCN + $Al_2O_3$ coating and 0.445 of the uncoated tools. This is attributed not only to the lower COF of PVD AlTiN, but also, to the nanoscale $Al_2O_3$ and $TiO_2$ tribo-films that form and improve the frictional conditions between the tool and the workpiece, along with the chemical stability of the cutting tool (33).

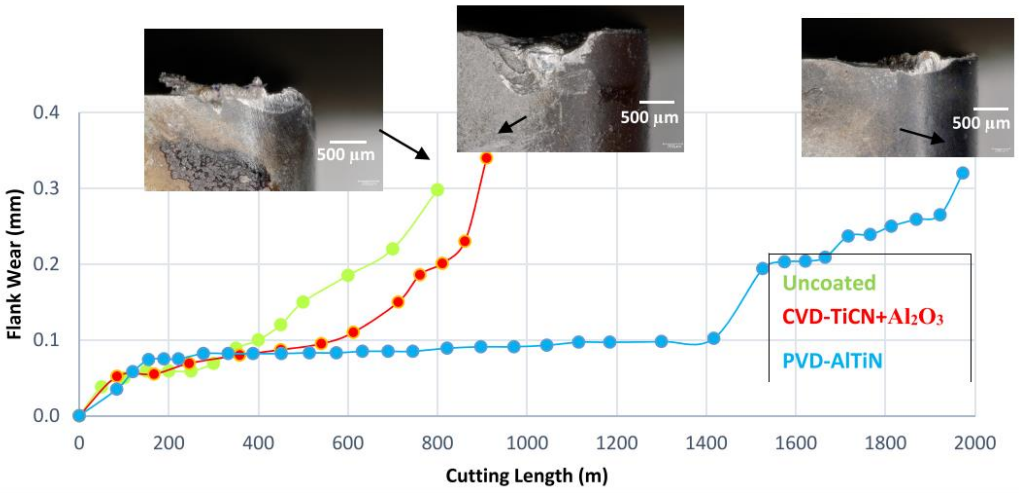


*Figure 14. Flank wear measurements for machining S32750 using uncoated, CVD and PVD coated tools. Used with permission* (33).

Tribo-films are formed as a result of the adaptation of the coating material as a response to external impact, which is thermodynamically far from equilibrium and favors the spontaneous formation of self-organizing secondary structures (32).

The most common technique to measure the coefficient of friction is called pin-on-disk, where the magnitude of COF is measured from the contact between two surfaces under a specified load, linear velocity and sliding distance. It is ultimately defined by the ratio of the moving force to the applied load (9,26). This method was used to investigate the tribological behavior of S32750 against different PVD coatings applied on cemented carbide tools. By comparing the COF curves extracted from experiments under dry and lubricated conditions, one can clearly see the difference. In this application $Al_{50}Cr_{50}N$ + $Ti_{95}Si_5N$ performed best in terms of friction behavior (9).

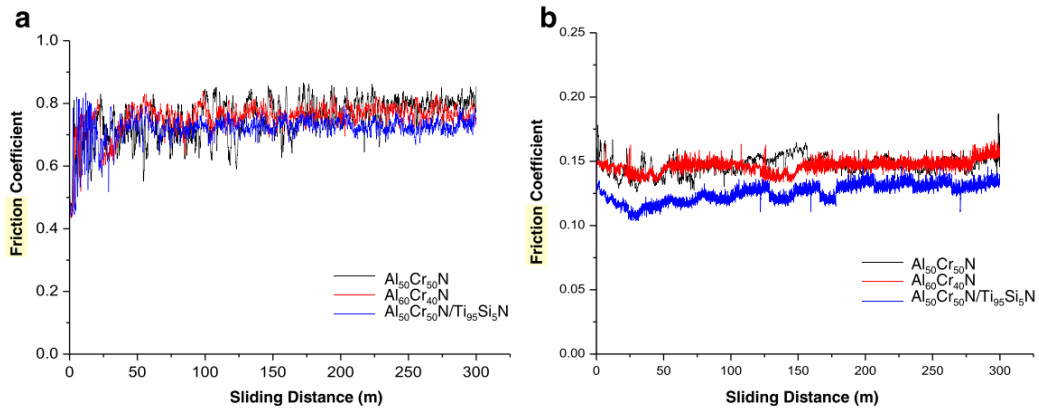


*Figure 15. Coefficient of friction curves for different PVD coatings against S32750 under dry (a) and lubricated (b) conditions. Used with permission* (9).

*Chemical stability*

High cutting temperature and great affinity between the chemical constituents of the workpiece, the tool and even the coolant/lubricant can lead to aggravated wear, which can take place from different mechanisms, such as adhesion, oxidation, diffusion and corrosion. The correct application of coated tools can provide additional resistance to these

mechanisms and, consequently, reduce tool wear (27). This enhancement can be attributed to the formation of tribo-films such as titanium, aluminum and chromium oxides which are chemically stable up to very high temperatures (32).

*Residual stress*

When materials are processed the intrinsic changes in their microstructure combined with temperature changes originate a stress on the surface of these materials. This stress remains on the surface even if no external load is being applied. For coatings, the coefficient of thermal expansion mismatch between the coating and the substrate leads to thermal stress and the structure/morphology of the coating is responsible for the intrinsic stress contribution. The residual stress can be of two types, compressive and tensile. Compressive stress happens when the surface/coating wants to expand while the substrate compresses it to remain with the same dimensions. The opposite is valid for tensile stress. The compressive is most desirable because it enhances the wear resistance of the coating because it increases crack propagation resistance, whereas tensile stress can lead to coating delamination (6,30).

However, there is a limit for compressive residual stress that should be assessed for each application. It is not a rule of thumb that the higher the compressive stress the more wear resistant the coating is. In many cases, due to the tool geometry the compressive stresses can accumulate and lead to delamination just as much as tensile stress would. Not to mention issues such as spallation and micro breakage. The residual stress is the one of the reasons why thick coatings are not as effective as thin coatings due to coating

delamination and premature tool failure. Therefore, for optimal coating performance, the compressive residual stress is usually kept in the range of 0.1 to 4 GPa (6,30).

Adhesion

The bond between the coating and the substrate must be strong enough to withstand the loads caused by metal cutting, not to mention, the BUE formation. Otherwise, the coating fails and delaminates, leaving the substrate exposed, which accelerates tool wear. The science behind this property is very complex, for adhesion depends on many factors, such as residual stress, substrate roughness, interface chemistry, surface contaminants, mismatch of elastic modulus and coefficient of thermal expansion and deposition parameters (6,26,27,30,32).

As previously mentioned, when machining S32750 SDSS, it is expected that intense heat is generated within the cutting zone, which leads to accelerated tool wear by temperature-associated mechanisms (diffusion, adhesion, oxidation, etc.). Another issue related to the machining of S32750 is related to the work hardening of the workpiece, as a consequence, higher cutting forces are applied. Therefore, the bond between the coating and the substrate must be optimized to endure harsh conditions.

### 2.4.6. Coatings for machining S32750 SDSS

In one study, Lima showed that PVD AlTiN/$TiB_2$ cutting inserts performed better than tools coated with PVD AlTiN and AlTiN / WC/C, with respect to tool life, for the finish turning of S32750 at 110 m/min. And, at higher cutting speed (130 m/min) the bi-

layer PVD CrN/AlTiN coating outperformed PVD AlTiN/$TiB_2$, PVD AlTiN and PVD AlTiN/CrN (7).

Parsi et al. evaluated PVD AlTiN and AlCrN coated turning inserts for the machining of S32750 at 100 and 140 m/min and the formation of Al-Cr and Al-Ti tribofilms. In both cases, PVD AlTiN showed longer tool life. The author states that Al-Cr tribo-oxides promote resistance to abrasion, while Al-Ti tribo-oxides are less reactive with the substrate, which improves the resistance to adhesive wear (8). Similarly, Junior investigated the machining behavior of PVD AlTiN, AlCrN and AlCrN/TiSiN coated carbide inserts for the turning of S32750 at 120 m/min. PVD AlTiN coated tools cut two times the length than the other coated tools before failure. The author attributed the performance of PVD AlTiN to lower friction conditions (lower roughness and lower work-hardening of the machined surface) and the increased thermal-barrier effect (higher residual stress of the workpiece) (36).

Ahmed et al. compared PVD AlTiN and CVD TiCN+Al2O3 coated inserts for the rough turning of S32750 and concluded that PVD AlTiN performed better due to better friction condition in the cutting zone (between the chip and the rake face). Aluminum oxide tribo-films were associated with reduced BUE formation and crater wear, as well as, higher resistance to adhesion and chipping (33). In a similar study, Martinho et al. compared monolayer PVD AlTiN and multilayer CVD TiN/TiCN/$Al_2O_3$ coated cutting inserts for the dry milling of a duplex grade stainless steel workpiece. The authors suggest that PVD AlTiN is more suitable for finishing operations by comparing the roughness of the machined surfaces. On the other hand, CVD TiN/TiCN/$Al_2O_3$ shows better wear resistance

due to increased thickness and, therefore, is recommended for roughing operations (34). Sousa et al. linked the performance of PVD TiAlN, AlCrN and TiAlSiN coated milling tools during the machining of S32101 duplex stainless steel to their mechanical properties. In this study, the tools coated with TiAlSiN promoted better workpiece surface integrity with higher resistance to wear due to high values of H/E and $H^3/E^2$ ratios, as well as lower $E_c/E_s$ ratio (37).

Paiva et al. studied the tribological behavior of S32750 pins against coated WC/Co disks. The performance of different AlCrN coatings was analyzed and the multilayer $Al_{50}Cr_{50}N$ / $Ti_{95}Si_5N$ showed lower friction and wear rate of the S32750 pins in comparison to monolayers $Al_{50}Cr_{50}N$ and $Al_{60}Cr_{40}N$ (9).

# 3. METHODOLOGY

## 3.1. Overview

This study was conducted in two distinct fronts, machining experiments and the characterization of the coatings.

Two turning experiments were carried out to compare the tool life and wear mechanisms through measurements of the rake and flank wear. The acquisition of the cutting forces included in the turning tests to support the data on the performance of the cutting tools. To examine chip formation, data on morphology, undersurface roughness, shear band was collected. The machined surface integrity will be evaluated using microhardness and roughness measurements.

Experiment 1 was conducted to evaluate the wear performance of the uncoated tool and the Certiphy (TiAlN - HIPIMS) coated tool to establish a baseline of performance and the industry standard, respectively. The coatings that were selected for this experiment were Fortiphy (CrN – HiPIMS), Croma Plus (Cr + CrN + OX – Arc), Formera (CrN + CrTiAlN - Arc), Alcronos (AlCrN – HiPIMS) and Alnova (AlCrN + AlCrSiN - Arc).

Experiment 2 consisted of longer passes for more aggressive cutting conditions. The wear behavior of Alcronos, Alnova and Alcrona Pro (AlCrN – Arc) was evaluated.

Coated test coupons were used to characterize the coatings with respect to morphological, mechanical and tribological properties. The data about chemical composition, phase analysis, thickness, and residual stress provide valuable information on the nature of the selected coatings, while their mechanical properties such as hardness,

elastic modulus and adhesion can be correlated with the coating performance during the machining tests.

## 3.2. Wear performance evaluation

### 3.2.1. Machining setup

The machining tests were conducted on the Nakamura-SC450 lathe. The cutting parameters used were speed: 150 m/min; feed rate: 0.15mm/rev; depth of cut: 0.5 mm and flood coolant: CommCool 8800 at 12 L/min and 6% concentration. The length of the pass is 100 ±10 mm for experiment 1 and 200 ±10 mm for experiment 2. These parameters were defined based on literature review (5,7–9,33,34,36,37) .The cutting forces measurements in the range of -3kN to 3kN were taken from the quartz dynamometer Kistler 9121 with a natural frequency of 10kHz attached to the tool holder. The setup is illustrated in Figure 16.

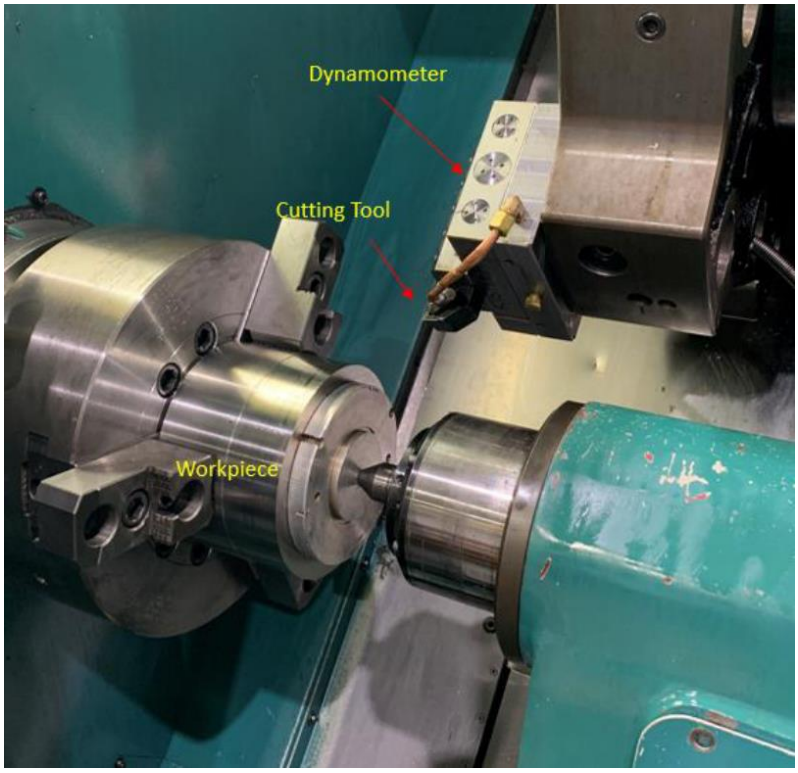


*Figure 16. Experimental setup for the machining wear performance tests.*

### 3.2.2. Workpiece

The super duplex stainless steel used in this research is the UNS S32750 grade manufactured by Vallourec Tube Solutions of Brazil (see Figure 17).

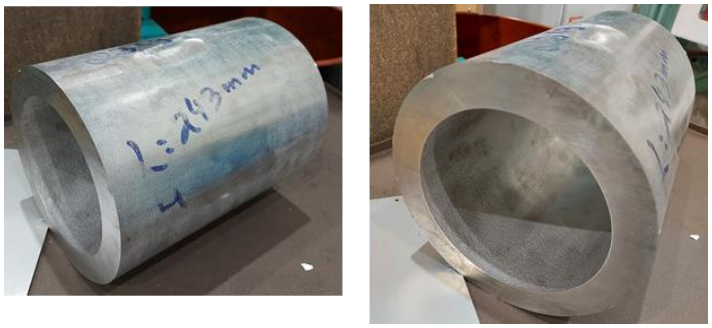

*Figure 17. S32750 workpiece.*

The chemical composition is given in Table 4. The corresponding $PRE_N$ number is 43 and the dual microstructure consisted of 48% austenite and 52% ferrite phases is revealed in Figure 1.

*Table 4. Chemical composition of the S32750 workpiece. Provided by the manufacturer.*

| **Element** | **Cr** | **Mo** | **N** | **Ni** | **C** | **Mn** | **Si** | **Cu** | **P** | **S** | **Fe** |
|---|---|---|---|---|---|---|---|---|---|---|---|
| **Weight (%)** | 25 | 4 | 0.3 | 7 | 0.03 | 1.13 | 0.65 | 0.78 | 0.0012 | 0.018 | balance |

### 3.2.3. Cutting tool

The Kennametal CNGG120408FS K313 (CNGG 432FS) finishing sharp cutting insert was selected in this study. Rake angle: 10º; Flank angle: 1º; Edge angle: 79º; Nose radius: 0.8 mm; Edge radius: 15µm; Inscribed circle: 12.7 mm; Cutting edge length: 12.9 mm.

### 3.2.4. Tool wear measurements

The flank wear was measured using Keyence VHX-6000 optical microscope after each pass using 200x magnification. The volumetric crater wear was monitored and measured using the white light interferometer Alicona InfinityFocus. The chosen end of tool life criterion was 300µm of flank wear/chipping based on ISO standard 3685.

### 3.2.5. Chip analysis

Cross-section and undersurface examination of the chips produced in the first pass during the wear performance tests was carried out using a JEOL-6610 scanning electron microscope (SEM). The characterization of the chips with regards to chip compression ratio, shear angle and velocity was based on the principles proposed by Shaw (19).

### 3.2.6. Workpiece surface integrity

The surface roughness and the hardness profile were chosen as characterization methods for surface integrity. Sections of the workpiece were cut and cleaned in an ultrasonic bath with ethanol. The white light interferometer Alicona Infinite Focus was used to scan the surface samples. Areas of $1mm^2$ were randomly chosen and analyzed with 100x magnification. Due to the cylindrical shape of the workpiece, form corrections were applied to calculate the surface roughness.

For the microhardness profile, sections of the workpiece were mounted and prepared through metallography. Once the samples were prepared, the microhardness tester Matsuzawa model MMT-X with a Vickers indenter. 20 indentations were collected for each sample at load of 10g for 10s.

## 3.3. Coating characterization

### 3.3.1. Chemical composition, thickness and residual stress

Cross-section examination of the coated coupons was carried out using the JEOL-6610 scanning electron microscope (SEM) with Energy Dispersive Spectroscopy (EDS) to

study the chemical composition and thickness of the coatings. Residual stress data was collected by an X-ray diffractometer (XRD) using a Ti target at 30kV and 20mA with an elastic constant of 12200ksi, 80$^{o}$ Bragg angle and 20 exposures.

### 3.3.2. Tool topography, geometry and 3D profile imaging

The white light interferometry microscope Alicona InfiniteFocus was used to acquire surface topography data (such as roughness and texture) as well as tool geometry data (edge profile) and 3D volumetric wear measurements.

### 3.3.3. Mechanical properties and adhesion

The Anton-Paar USP - Nanoindention Tester model NHT$^{3}$ was used for the measurement of nano-hardness and elastic modulus. The tests were carried out in accordance with ISO 14577-4 by a calibrated Berkovich B-V 76 indenter. A linear load of 50mN was applied at the loading/unloading rate of 100mN/min with a 5 second pause. 20 measurements were taken.

To measure coating adhesion the Anton-Paar RST-3 Revetest scratch tester was used. The instrument was equipped with a diamond Rockwell AJ-259 indenter that has a radius of 200μm. The 3-scan progressive scratch mode was employed (pre-scan, progressive scratch and post-topography). The progressive scratch started with a 0.5N load and the final load was 180N with a 360N/min loading rate at 6mm/min for a total of 3mm in length. 3 scratches were performed on each sample.

# 4. RESULTS AND DISCUSSIONS

## 4.1. Wear Performance

### 4.1.1. Experiment 1

The tool wear curves (flank wear vs cutting length) are represented in Figure 18. Typically, these curves are composed of three regions. The tool wear begins in the first region at an accelerated rate due to changes in the tool geometry, more specifically, the new sharp cutting edge becomes rounded. As the cutting edge adapts, the wear rate slows down. The second region is where the tool tends to be worn at a lower and steady rate until the cutting edge is damaged to a critical level, the beginning of the failure region. At this point, flank wear is associated with crater wear and additional wear mechanisms can take place. Temperature rises and friction conditions become so aggressive that the tool fails abruptly. In this study, both AlCrN-based coatings, Alcronos and Alnova, had similar performance improving the cutting tool life significantly when compared to the uncoated tool, approximately 6 times. When compared to the selected TiAlN industry standard Certiphy, an improvement of about 70% in tool life can be observed. The CrN-based coatings Fortiphy and Croma Plus did not perform as well as the other coatings. Croma Plus offered very little protection and the tool wear progressed in a very similar fashion to the uncoated tool. Fortiphy resisted up to 800m of total cutting length when it lost integrity and the tool wear accelerated. Formera, also a CrN-based coating, had a very similar wear behavior to Certiphy undergoing progressive wear until failure, but the latter had marginally better performance throughout the entire experiment.

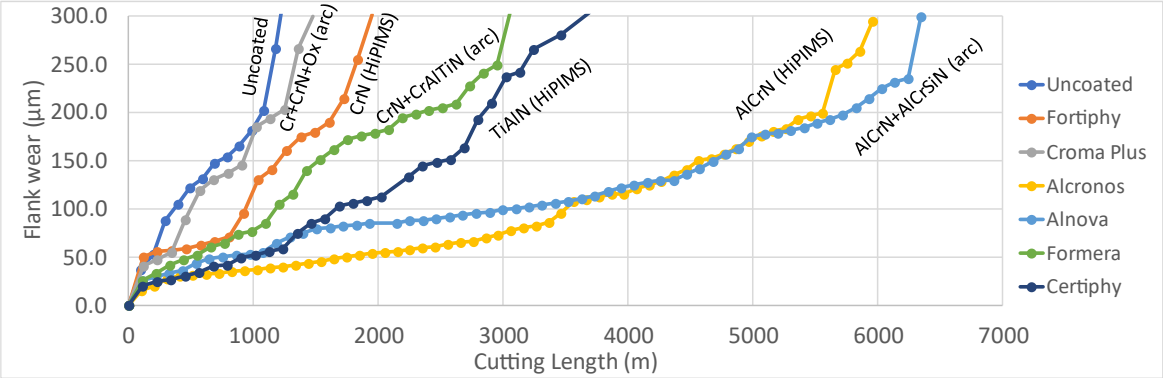


*Figure 18. Flank wear curves – Experiment 1*

### 4.1.2. Wear Mechanisms

When machining S32750 all tools experienced intense adhesion of the workpiece material on the flank and rake face (see Figure 19). The material accumulates mostly at the cutting edge, changing its dimension. This build-up edge formation causes instability in the cutting zone and when it snaps off, it takes away fragments of the cutting tool material with it leading to chipping and ultimately failure. The rake face is affected by strong adhesion combined with high compressive stress from chip formation which intensifies crater wear. Heat is not properly dissipated due to the low thermal conductivity of the workpiece which aggravates wear mechanisms such as oxidation and diffusion.

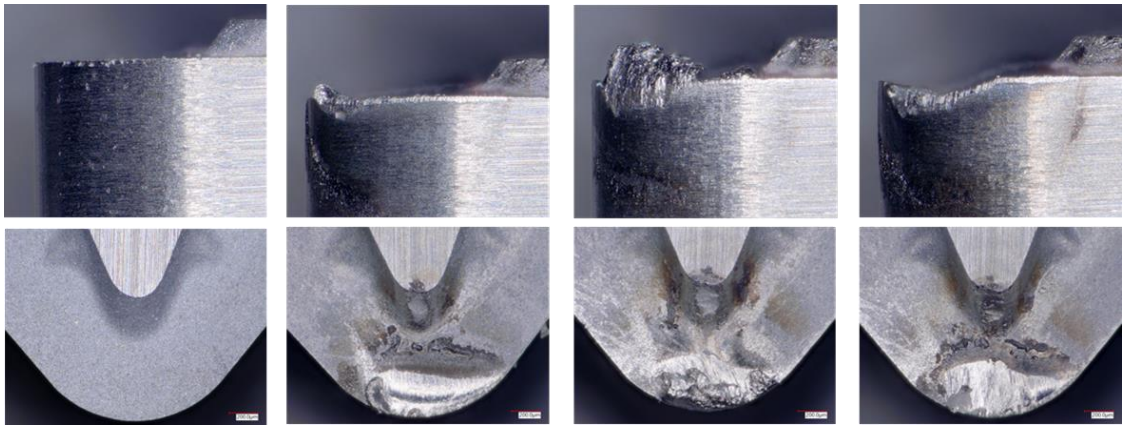

*Figure 19. Tool wear progression of the uncoated carbide insert within the initial 500m of cutting length.*

Ahmed et al. observed that when machining S32750 at high cutting speeds (150m/min) crater wear is intensified causing chipping and, consequently, rapid tool wear. Also, at high cutting speeds, BUE has reduced size in comparison to lower cutting speeds (5,33). Lima conducted similar machining experiments at 130m/min and reported that tools failed mainly due to intense crater wear (7). The evaluated AlCrN-based coatings are capable of withstanding these BUE formation cyclic events promoting better frictional conditions within the cutting zone and slowing down the wear rate of the tools. Images of the flank and rake faces of the coated tools after approximately 500m of cutting length are shown in Figure 20. Alcronos, Alnova and Certiphy have less material adhered to both the flank and rake which can be attributed to lower friction in the cutting zone and smoother flow of the chips that, in turn, allows for better heat dissipation, ultimately protecting the tool from excessive wear. Although, flank wear observed for Formera and Fortiphy are not significantly higher, the crater wear area is noticeably larger. The images indicate that

Croma Plus experienced severe frictional conditions from the beginning of the experiment, the chip breaker is damaged which can also affect the chip flow and aggravate temperature and friction related wear mechanisms.

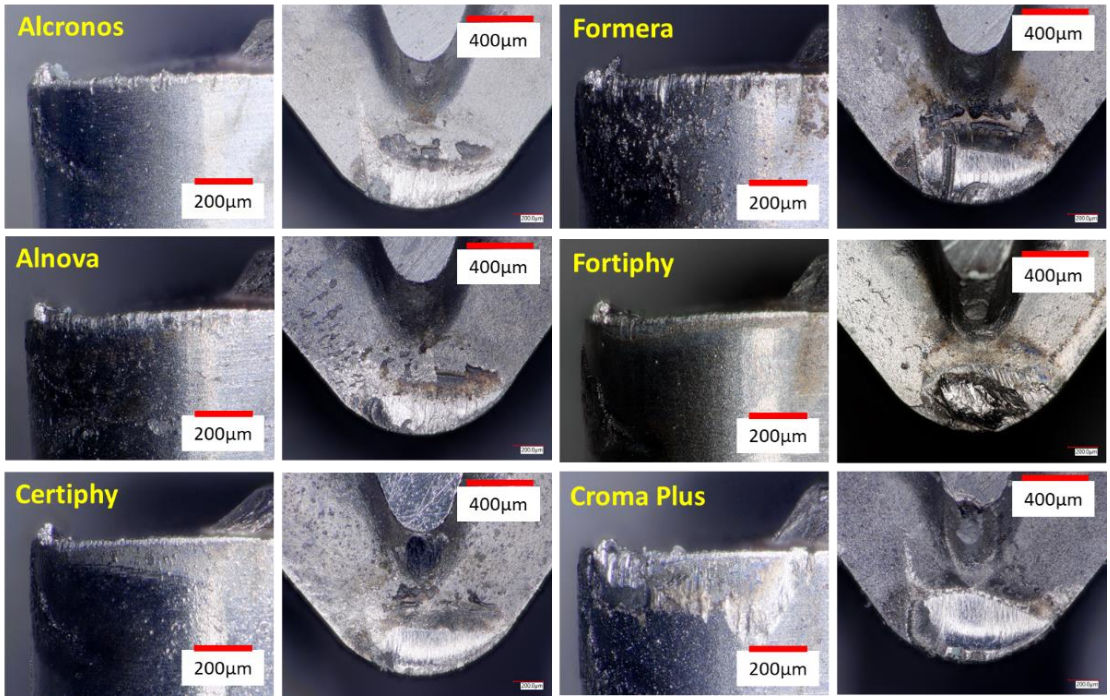


*Figure 20. Flank and rake faces of the coated tools after approximately 500m of cutting length.*

When coatings are exposed to high stresses, speed and temperature such as those generated under aggressive metal cutting conditions, the surface of the coatings can self-organize into oxide tribo-films. These newly formed oxides on the surface of the coating can provide additional wear resistance as they act as thermo-barriers reducing heat generation, or they might reduce the chemical affinity between the workpiece and tool which, in turn, reduces adhesion. Or they can even offer protection against abrasion (32).

Several types of tribo-films and their beneficial properties have been reported including Al-Cr and Al-Ti oxides (8), $Al_2O_3$ and $Ti_2O_3$ (33) $Cr_2O_3$ (38,39), $B_2O_3$ (40). The images from Figure 20 suggest that Alcronos, Alnova and Certiphy have the ability to produce more chemically stable tribofilms that prevent intense adhesion and BUE formation resulting in reduced crater wear. By examining the wear curves in Figure 18 it is also evident that Alcronos sustained better friction conditions throughout most of the cutting tests and, thus, lower wear.

### 4.1.3. Experiment 2

Experiment 2 (Figure 21) consisted of prolonging the exposure of the tools to the wear mechanisms through increasing the cutting length of each pass during the machining tests. As expected, the tool life of the tools coated with Alcronos and Alnova was reduced compared to Experiment 1. However, Alcronos performed significantly better than Alnova, which contradicts the findings in the previous experiment. An explanation for this could be that since severe chipping was the cause of tool failure, and Alnova was maintaining a similar performance to Alcronos, it is possible that an event of random chipping occurred causing catastrophic failure of the tool coated with Alnova. A repetition of this Experiment could confirm these findings. Also, a detailed study on the wear mechanisms could prove useful for understanding the events of random chippings and coating delamination.

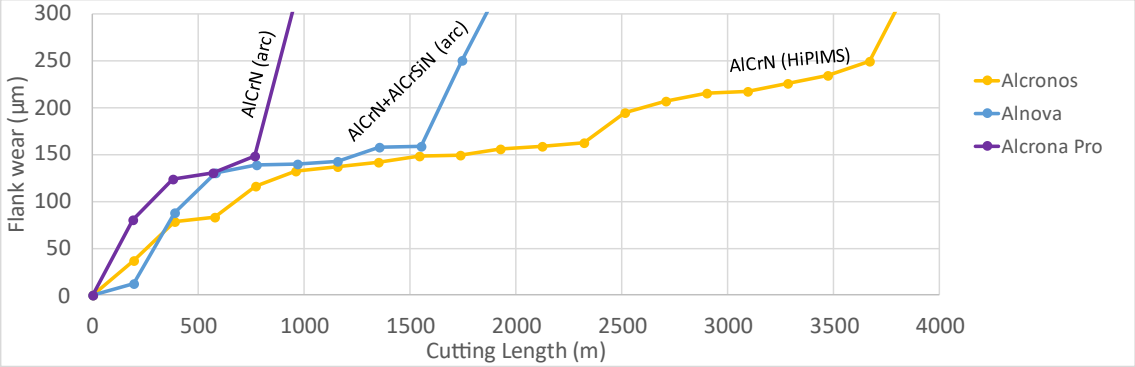


*Figure 21. Flank wear curves - Experiment 2*

The Alcrona Pro was introduced to this cutting experiment as an industrial benchmark and in order to evaluate the performance of AlCrN coatings with similar composition but deposited by different PVD methods. In this case, Alcronos was deposited using the HiPIMS technology which, in principle, produces denser coatings with better adhesion and less defects (26). When machining S32750 super duplex stainless steel, these coating properties can be crucial in achieving extended tool life which was supported by an almost 5 times longer life shown by the tool coated with Alcronos.

## 4.2. Cutting Force

The cutting forces can be related to several events during machining. For example, BUE formation and chipping may change the effective cutting edge leading to an increase in cutting forces. As the tool wear progresses it is expected that the cutting forces follow the same trend (5). The maximum tangential forces measurements during the first pass in Experiment 1 are represented in Figure 22. By analyzing the force in the beginning of the

cutting test it is possible to compare the behavior of the coating while they have full integrity.

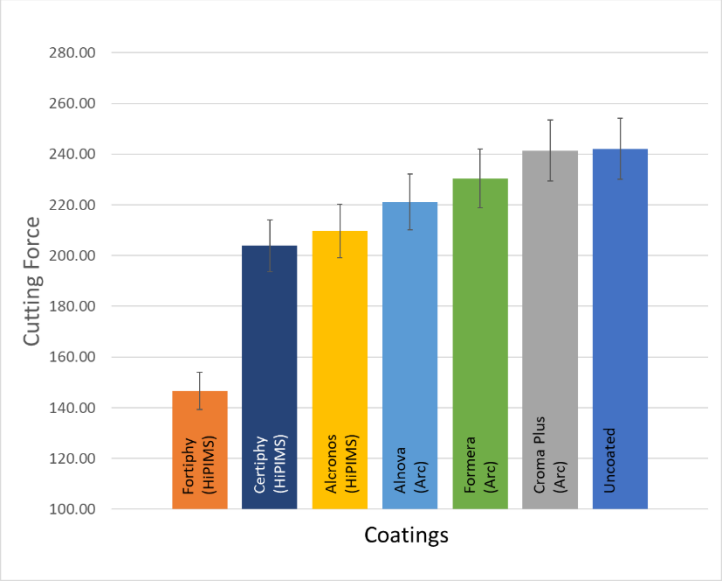


*Figure 22. Max tangential force at the first pass collected during Experiment 1.*

Alcronos, Fortiphy and Certiphy measured low cutting force during the first pass. It can be seen that the coatings produced by HiPIMS technology have the ability to better control the friction within the cutting zone. Nevertheless, other wear mechanisms also play an important role in the wear behavior of tools machining S32750, which is evidenced by the difference in flank and rake wear progression of these tools.

## 4.3. Chip Analysis

### 4.4.1. Chip Morphology and Undersurface Roughness

Long, curly, serrated chips were produced in all machining tests. The serrated chip formation occurs due to the low thermal conductivity of the S32750 SDSS associated with

high cutting speed. The length and curliness of the chips are commonly observed when machining ductile materials, especially stainless steels (41). Figure 23 contains SEM images of the chips produced by the tools coated with Alcronos, Alnova and Alcrona Pro. At 15x magnification it is possible to see that Alcronos and Alnova produced chips with more regular curliness when compared to Alcrona Pro. This indicates that the chip flows more irregularly over the rake face of the tools coated with Alcrona Pro (33,39,42). By examining the undersurface and the shear bands it is possible to have an insight into the friction conditions as well as the cutting forces on the chip generation. Alcronos and Alnova generated chips with smoother undersurface with less defects than Alcrona Pro. The more accentuated flow marks and defects that can be seen on the chips from Alcrona Pro suggest that when the chips are formed the friction at the tool/chip interface cause material from the chip to attach to the rake face and, as the chip flows, it tears and generates a rougher undersurface (33,39,42). The shear bands produced in the chips from Alcronos are less plastically deformed when compared to Alnova and Alcrona Pro. This can be related to the speed of the chip flow on Table 5. For rapid chip formation there is less time available for the material to strain harden and the shear bands become more well defined and with less defects (33,39,42).

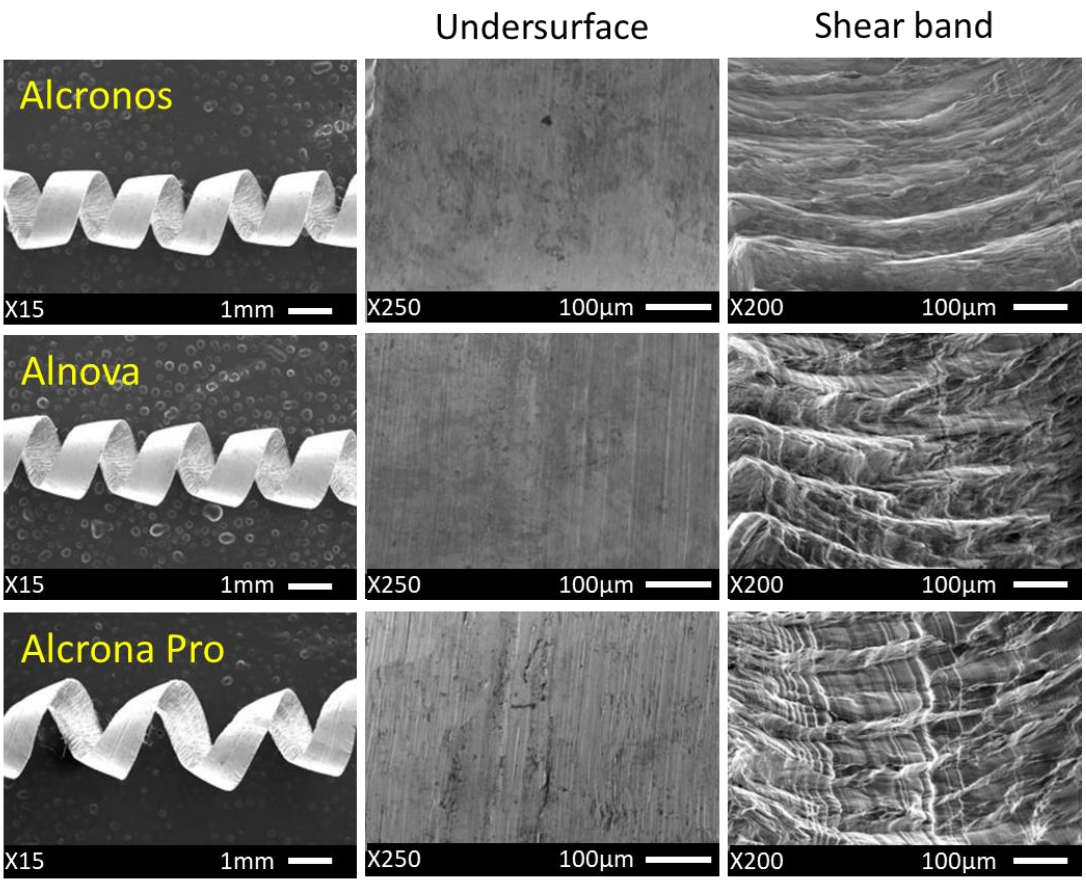


*Figure 23. SEM images of the morphology, undersurface and shear bands of the chips produced in Experiment 2.*

### 4.4.2. Chip characterization

Table 5 contains details on the chip characterization. Alcronos has thinner chips, and higher compression ratio, shear angle and speed indicating more favorable friction conditions and that the heat is dissipated with the chips more efficiently. The values for chip compression ratio and shear angle for Alcronos suggest reduced shearing force acting at the cutting edge and consequently lower friction at the tool/chip interface (33,39,42).

The chip also flows more rapidly when machining with Alcronos, which results in less contact between chip and tool allowing for better heat dissipation.

*Table 5. Chip characterization data.*

| | **Thickness (mm)** | **Compression Ratio** | **Φ Shear Angle (°)** | **Chip Velocity (m/min)** |
|---|---|---|---|---|
| **ALCRONOS** | 0.27 | 0.55 | 30.00 | 82.7 |
| **ALNOVA** | 0.29 | 0.52 | 28.47 | 77.9 |
| **ALCRONA PRO** | 0.33 | 0.45 | 25.29 | 68.3 |

## 4.4. Workpiece surface integrity

The data on surface roughness measured from the surface of the machined samples reveal a rougher finish for Certiphy in Experiment 1 and Alcrona Pro in Experiment 2 (see Figure 24). These results can be correlated with changes in the cutting edge radius due to BUE formation and adhesive wear causing ploughing and consequently a more irregular surface. A connection between the wear performance, chip flow and workpiece surface integrity can be drawn from the data presented in this study.

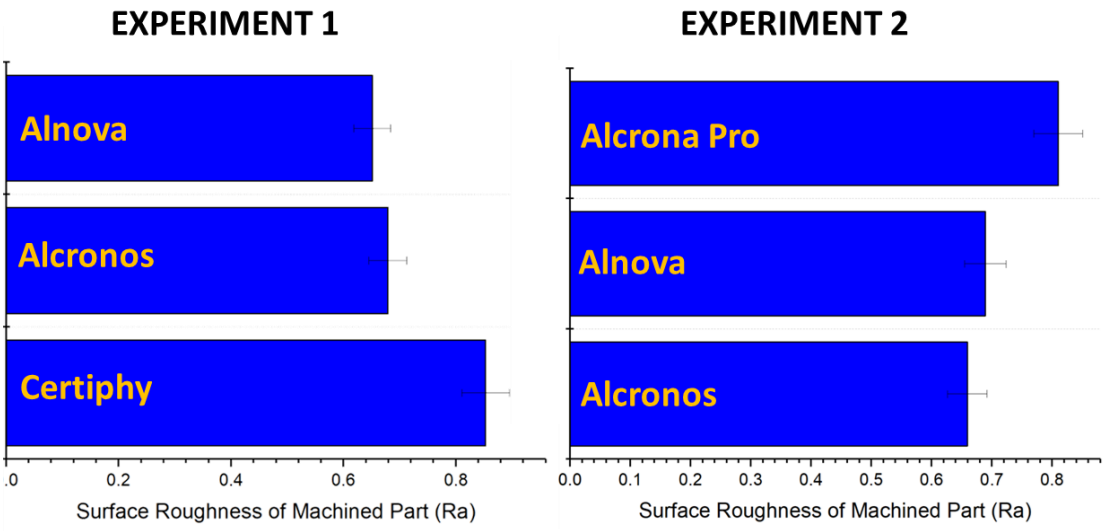


*Figure 24. Surface roughness of machined samples from Experiment 1 and 2.*

The microhardness profiles of the machined samples produced during Experiment 1 and 2 can be seen in Figure 25. It reveals the effect of machining on the subsurface of the workpiece. When machining with Alcronos and Alnova the strain hardening effects on the workpiece are reduced in comparison to Certiphy (Experiment 1) and Alcrona Pro (Experiment 2). Strain hardening can be detrimental for final product quality, and it can contribute to premature tool failure by affecting chip generation and friction at the tool/chip interface.

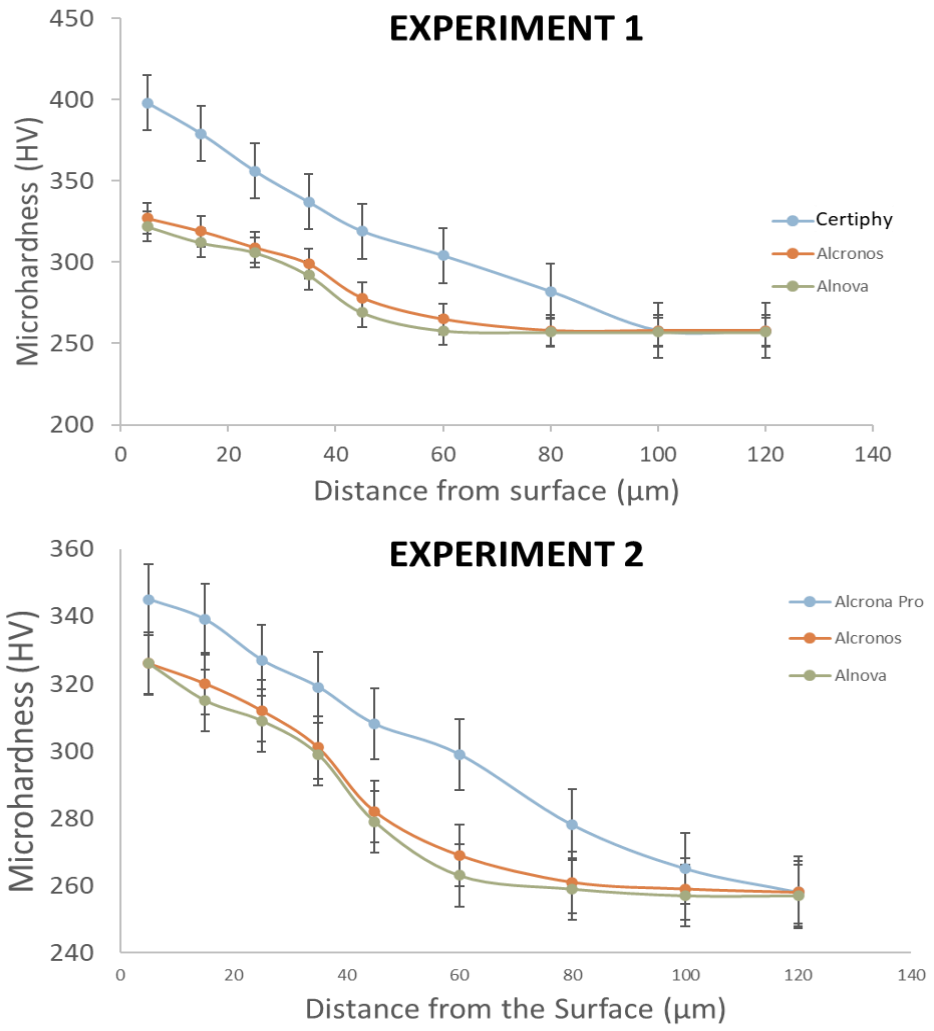


*Figure 25. Microhardness profile of machined surface samples from Experiment 1 and 2.*

## 4.5. Coating Properties

### 4.6.1. Micromechanical properties

From Table 6 it can be seen that Alcronos and Alnova have the lowest thickness values (3μm), followed by Certiphy (4μm), Formera (5μm), Fortiphy (6μm) and Croma Plus (13μm). In Experiment 1, the thicker coatings such as Formera, Fortiphy and Croma had lower performance (see Figure 18) an increased thickness leads to high internal residual stresses and when exposed to high pressure, friction and temperature generated under cutting conditions these stresses can favor the formation and propagation of internal cracks and interlayer delamination, resulting in catastrophic failure (43). Therefore, the performance of Croma Plus, Fortiphy and Formera might have been severely impacted by their increased thickness. In Experiment 2 (see Figure 21), three coatings with roughly the same thicknesses were tested under prolonged exposure to cutting conditions. Alcronos promoted increased tool life when tested against Alnova and Alcrona Pro. Indicating that, although coating thickness can affect tool geometry and consequently forces and friction within the cutting zone, the machining performance is also interrelated with other coating properties. The task of finding the best candidate for a specific machining operation involves identifying the most suitable combination of micromechanical properties for that particular application.

*Table 6. Micromechanical properties*

| Coating | Material | Deposition method | Thickness (µm) | Hardness (GPa) | Elastic Modulus (GPa) |
|---|---|---|---|---|---|
| **ALCRONOS** | **AlCrN** | HiPIMS | 3+/-0.5 | 36.5 +/- 2.6 | 384 +/- 29 |
| **ALNOVA** | **AlCrN+AlCrSiN** | Arc | 3+/-0.5 | 38.4+/- 2.4 | 370 +/- 29 |
| **CERTIPHY** | **TiAlN** | HiPIMS | 4+/-0.5 | 34.8 +/- 2.4 | 346 +/- 29 |
| **FORMERA** | **CrN+CrAlTiN** | Arc | 5+/-0.5 | 28.3 +/- 3.2 | 337 +/- 28 |
| **FORTIPHY** | **CrN** | HiPIMS | 6+/-0.5 | 23.4 +/- 2.1 | 294 +/- 21 |
| **CROMA PLUS** | **Cr + CrN + OX** | Arc | 13+/-1.0 | 31.4 +/- 6.2 | 282 +/- 39 |

| Coating | H/E | $H^3/E^2$ | Plasticity Index | Adhesive Failure Lc2 (N) | Critical Load Lc3 (N) |
|---|---|---|---|---|---|
| **ALCRONOS** | 0.096 | 0.341 | 0.364 | 56.2 | 139.3 |
| **ALNOVA** | 0.104 | 0.425 | 0.325 | 61.3 | 109.7 |
| **CERTIPHY** | 0.104 | 0.379 | 0.346 | 90.1 | 111.1 |
| **FORMERA** | 0.084 | 0.206 | 0.477 | 72.5 | 93.0 |
| **FORTIPHY** | 0.080 | 0.155 | 0.541 | 89.1 | 120.7 |
| **CROMA PLUS** | 0.111 | 0.417 | 0.331 | - | - |

The hardness of the coating can be related to wear resistance, while the ratios H/E and $H^3/E^2$ are connected with the elastic strain to failure and the resistance to plastic deformation. In combination, with the plasticity index that reflects the ability of the material to dissipate loads, these properties can provide a good insight into the coatings resilience and the set of requirements imposed by the cutting conditions (32,38,40,44,45). AlCrN-based coatings are harder in comparison to CrN and have similar hardness to TiAlN. Croma Plus has a top chromium oxide layer that has high hardness but low elasticity which

indicates that the surface of this coating is very brittle. Alcronos has a higher elastic modulus than Alnova and Certiphy and, consequently, lower H/E and $H^3/E^2$ ratios. Additionally, Alcronos has higher plasticity index value which suggests that Alcronos is tougher among them and has better capability of dissipating the energy that is generated through friction.

Chowdhury et al. compared the wear performance of TiAlN and $TiB_2$ coated inserts for the machining of $Ti_6Al_4V$ alloy. The authors found that $TiB_2$ promotes better wear resistance with lower H/E and $H^3/E^2$ ratios but higher plasticity index value (40). In another study Chowdhury analyzed the wear behavior of CrN and AlTiN coated inserts for the machining of the same Ti alloy. CrN outperformed AlTiN that has higher values of H/E and $H^3/E^2$ ratios and lower plasticity index (38). Lima tested AlTiN + $TiB_2$ and AlTiN + WC/C multilayered coatings for the machining of super duplex stainless steel against the monolayer AlTiN. The wear results show superior resistance for AlTiN + $TiB_2$ which is also the coating with lowest H/E ratio (7).

The progressive scratch test can provide useful information on the response of the coating to different loads. By applying a progressive load, it is possible to verify the coating failure mechanisms. Coatings fail firstly cohesively (Lc1-elastic deformation) before the adhesive failure occurs (Lc2-onset of plastic deformation) leading to total substrate exposure (Lc3-catastrophic failure) (32,40,44,45). Values of Lc2 and Lc1 can be found on Table 6, the results show that Alcronos can withstand more plastic deformation and the coating fails at the highest load among the compared coatings. This might reflect the ability of the coating to withstand crack propagation. Fortiphy showed higher Lc2 and Lc3 which

might indicate good adhesion to the carbide substrate and capability of dissipating the progressive load, this can be linked to its low H/E, $H^3/E^2$ and high PI values.

By looking at the SEM images of the scratch marks on Alcronos and Alnova shown in Figure 26 it is possible to appreciate the difference between the failure modes of both coatings. The spallation begins at roughly the same load, however, Alcronos is able to withstand more plastic deformation and total delamination occurs later. The chipping and spallation seen on Alnova's scratches are more aggressive causing total delamination of the coating in a larger area. Although machining conditions are far different from the scratch testing, it is important to understand the behavior of the coating under such conditions to establish a connection with the other micromechanical properties and the wear resistance of the coating for a specific process.

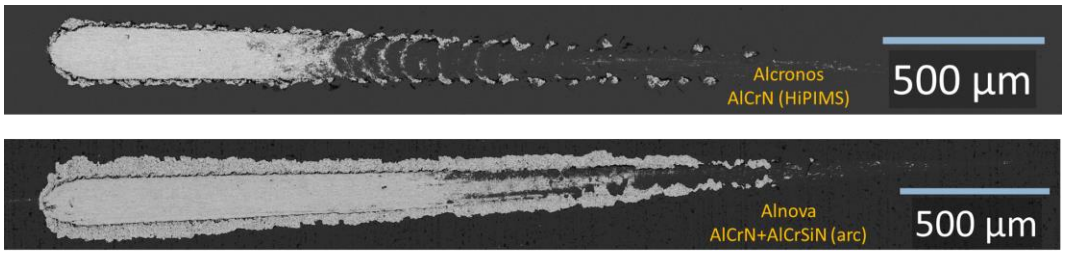


*Figure 26. Scratch images*

### 4.6.2. Composition and Phases

It can be seen from the SEM images of the coating cross-sections (Figure 27) that the HiPIMS technology is capable of producing coatings with less surface defects (microdroplets) and smoother surface. The approximate composition of the coatings was

measured using SEM-EDS (Table 7), Alcronos has higher Al content than Alnova. In addition, it was possible to detect traces of Si added as a doping agent to improve tribological properties of Alnova. The content of Al in Certiphy is also slightly higher than Ti.

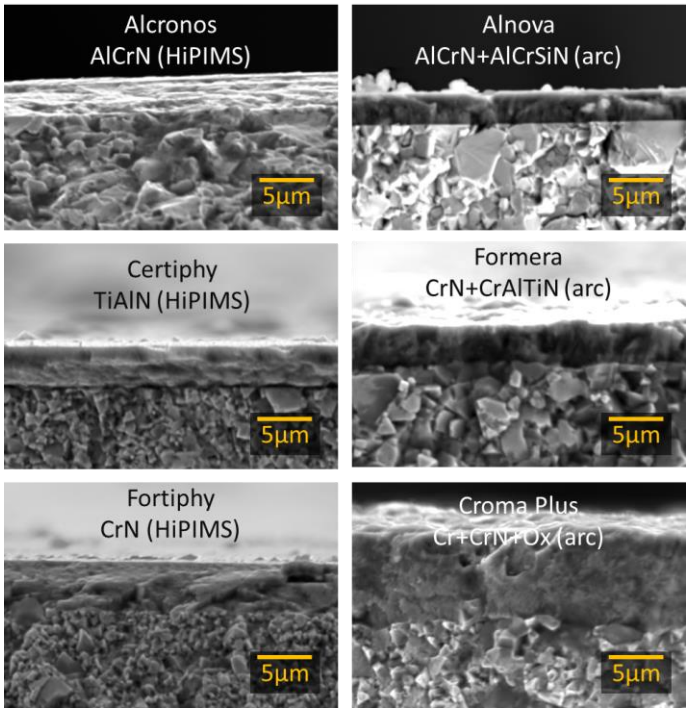


*Figure 27. SEM images of the cross-section of the coated coupons.*

*Table 7. EDS composition data of Alcronos, Alnova and Certiphy*

| Coating | Al/N | Cr/N | Ti/N | Si |
|---|---|---|---|---|
| **ALCRONOS** | 60% | 40% | | |
| **ALNOVA** | 50% | 50% | | >1% |
| **CERTIPHY** | 55% | | 45% | |

The XRD patterns shown in Figure 28 show clearly (111) (200) and (121) AlCrN peaks for Alcronos and Alnova. The higher intensity of peak (111) for Alcronos indicates preferred orientation (38,40). For Certiphy, (111), (200) and (220) TiAlN peaks can be observed.

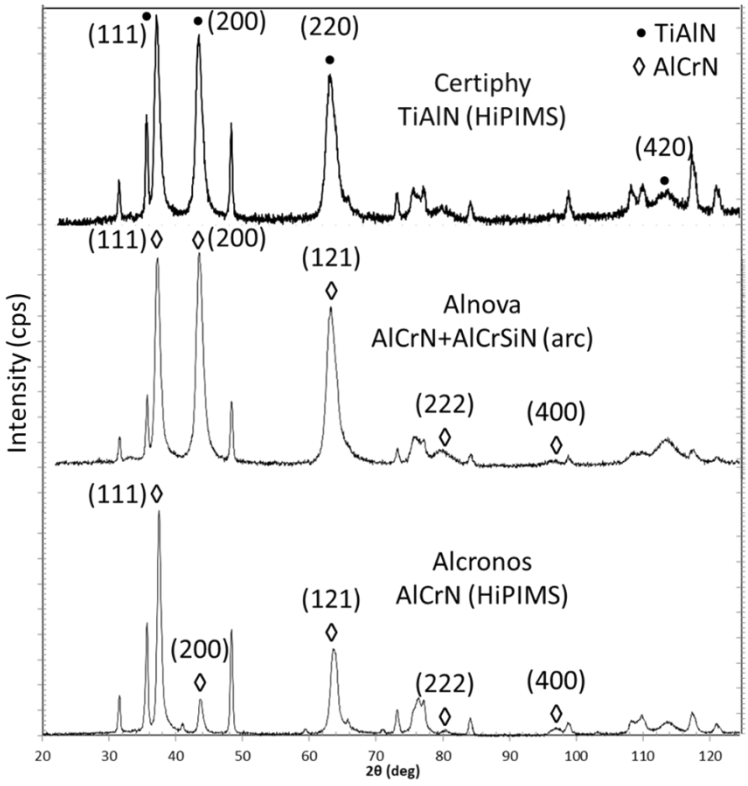


*Figure 28.XRD patterns collected for Alcronos, Alnova and Certiphy.*

# 5. CONCLUSIONS

The machining experiments combined with the cutting force, chip and workpiece surface integrity analysis provide good insight into the wear behavior of the selected coated carbide inserts compared in this study. The tool wear data can be correlated with the coating properties for a better understanding of the relation between coated tool and the workpiece material during cutting.

The tools fail by chipping and the major wear mechanisms were adhesion and BUE formation. Abrasion and oxidation were observed to take place mainly at the end of tool life.

AlCrN-based coatings improved tool life significantly in Experiment 1. About 5 to 6x longer than the uncoated tool and 70% longer than TiAlN in Experiment 1. For prolonged cutting passes, in Experiment 2, Alcronos outperformed Alnova doubling the tool life.

Alcronos and Alnova combine good micro-mechanical properties with the capability of self-organizing surface layers to produce protective lubricious tribo-films. They also improve tool wear resistance by providing chemical stability and high oxidation resistance. Collectively these effectively reduce BUE formation.

When machining with Alcronos and Alnova, the friction conditions in the cutting zone are improved. This can be seen through the cutting forces, workpiece surface integrity, chip morphology, undersurface characteristics and shear deformation.

# 6. SUGGESTIONS FOR FUTURE WORK

Taking into consideration the conclusions drawn from the present work, here is a list of suggested topics for future studies and research:

The effect of the coating thickness on tool geometry wear performance of coated AlCrN, CrN and TiAlN cutting tools.

The evaluation of the wear behavior of Alcronos and Alnova at different cutting speeds and feed rates to validate the performance of both coatings for roughing and finishing.

The evaluation of the wear performance of Alcronos and Alnova for milling and drilling operations.

The addition of a top CrN or AlCrN layer on TiAlN to study the wear behavior and coating properties of multilayered coatings for the machining of S32750.

# REFERENCES

1. Gunn RN. Duplex Stainless Steels - microstructure, properties and appications. Cambridge: Abington Publishing; 2003. 219 p.
2. Alvarez-Armas I, Degallaix-Moreuil S. Duplex stainless steels. Armas IA, Moreuil SD, editors. Vol. 41, Springs. 2009. 59–63 p.
3. Youssef HA. Machining of Stainless Steels and Super Alloys. Machining of Stainless Steels and Super Alloys. 2015.
4. Nomani J, Pramanik A, Hilditch T, Littlefair G. Machinability study of first generation duplex (2205), second generation duplex (2507) and austenite stainless steel during drilling process. Wear [Internet]. 2013;304(1–2):20–8. Available from: http://dx.doi.org/10.1016/j.wear.2013.04.008
5. Ahmed YS, Paiva JM, Bose B, Veldhuis SC. New observations on built-up edge structures for improving machining performance during the cutting of superduplex stainless steel. Tribol Int [Internet]. 2019;137(April):212–27. Available from: https://doi.org/10.1016/j.triboint.2019.04.039
6. Holmberg K, Matthews A. Coatings Tribology. Properties, Mechanisms, Techniques and Applications in Surface Engineering Vol 56. 2nd ed. Briscoe B, editor. Elsevier; 2009. 576 p.
7. Lima LM. A STUDY OF PVD BI-LAYER CUTTING TOOL COATINGS USED FOR MACHINING OF SUPER DUPLEX STAINLESS STEEL A STUDY OF PVD BI-LAYER CUTTING TOOL COATINGS USED FOR MACHINING OF SUPER DUPLEX STAINLESS STEEL. McMaster University; 2020.
8. Parsi PK, Kotha RS, Routhu T, Pandey S, Dwivedy M. Machinability evaluation of coated

carbide inserts in turning of super-duplex stainless steel. SN Appl Sci [Internet]. 2020;2(11):1–19. Available from: https://doi.org/10.1007/s42452-020-03570-9

9. Paiva JMF, Amorim FL, Soares PC, Veldhuis SC, Mendes LA, Torres RD. Tribological behavior of superduplex stainless steel against PVD hard coatings on cemented carbide. Int J Adv Manuf Technol. 2017;90(5–8):1649–58.
10. McGuire MF. Stainless Steels for Design Engineers. Stainless Steels for Design Engineers. 2008.
11. Pohl M, Storz O, Glogowski T. Effect of intermetallic precipitations on the properties of duplex stainless steel. Mater Charact. 2007;58(1):65–71.
12. (IMOA) IMA. Practical Guidelines for the Fabrication of. 2009. 1–64 p.
13. Nilsson JO. Super duplex stainless steels. Mater Sci Technol (United Kingdom). 1992;8(8):685–700.
14. Charles J. Composition and Properties of Duplex Stainless Steels. Pergamon. 1995;36:43–54.
15. Trent EM, Wright PK. Metal-Cutting. Fourth. Butterworth–Heinemann. 2000.
16. Stephenson DA, Agapiou JS. Metal Cutting Theory and Practice. Third. CRC Press; 2016.
17. Kishawy HA, Hosseini A. Machining Difficult-to-Cut Materials - Basic Principles and Challenges. First. J. Paulo Davim, editor. Cham: Springer Nature Switzerland; 2019.
18. Youssef H, El-Hofy H. Traditional Machining Technology. 2nd ed. Boca Raton: CRC Press; 2020. 474 p.
19. Shaw MC. Metal Cutting Principles. Second. Oxford University Press. 2005.
20. Mehta NK. Metal Cutting and Design of Cutting Tools, Jigs & Fixtures. McGraw Hill Education (India). 2015.
21. Davim JP, editor. Measurement in Machining and Tribology [Internet]. First. Cham:

Springer Nature Switzerland; 2019. 154 p. Available from: http://www.springer.com/series/11181

22. Sambedana S, Subhash N, Nithin Raj P, Jagadeesha T. Experimental Study on Surface Roughness and Optimization of Process Parameters Using ANN-GA in Milling of Super-Duplex Stainless Steel Under Dry and Wet Conditions [Internet]. Lecture Notes in Mechanical Engineering. Springer Singapore; 2019. 399–409 p. Available from: http://dx.doi.org/10.1007/978-981-13-6374-0_47
23. Kumar KS, Senthilkumaar JS, Thirumalai R. CHIP MORPHOLOGY INVESTIGATION AMONG DRY, WET AND GAS COOLED MACHINING OF SUPER DUPLEX STAINLESS STEEL. Appl Mech Mater. 2014;592–594(Imec 2014):811–5.
24. Nomani J, Pramanik A, Hilditch T, Littlefair G. Chip formation mechanism and machinability of wrought duplex stainless steel alloys. Int J Adv Manuf Technol. 2015;80(5–8):1127–35.
25. Gamarra JR, Diniz AE. Taper turning of super duplex stainless steel: tool life, tool wear and workpiece surface roughness. J Brazilian Soc Mech Sci Eng. 2018;40(1):1–13.
26. Mattox DM. Handbook of Physical Vapor Deposition (PVD) Processing [Internet]. 2nd ed. Elsevier; 2010. 746 p. Available from: http://www.elsevier.com/wps/find/bookdescription.cws_home/717814/description#description
27. Martin PM. Introduction to Surface Engineering and Functionally Engineered Materials. Introduction to Surface Engineering and Functionally Engineered Materials. 2011.
28. Katiyar JK, Ramkumar P, Rao TVVLN, Davim JP, editors. Tribology in Materials and Applications. First. Cham: Springer Nature Switzerland; 2020. 298 p.
29. Böhlmark J. Fundamentals of High Power Impulse Magnetron Sputtering [Internet].

Linköping Studies in Science and Technology. 2005. Available from: http://liu.diva-portal.org/smash/get/diva2:22370/FULLTEXT01

30. Takadoum J. Materials and Surface Engineering in Tribology. ISTE; 2008. 148–162 p.
31. Davim JP, editor. Tribology in Manufacturing Technology. Springer. 2013. 200 p.
32. Fox-Rabinovich GS, Totten GE. Self-organization during friction: Advanced surface-engineered materials and systems design. Self-Organization During Friction: Advanced Surface-Engineered Materials and Systems Design. 2006. 1–461 p.
33. Ahmed YS, Paiva JM, Covelli D, Veldhuis SC. Investigation of coated cutting tool performance during machining of super duplex stainless steels through 3DWear evaluations. Coatings. 2017;7(8).
34. Martinho RP, Silva FJG, Martins C, Lopes H. Comparative study of PVD and CVD cutting tools performance in milling of duplex stainless steel. Int J Adv Manuf Technol. 2019;102(5–8):2423–39.
35. Bouzakis KD, Michailidis N, Skordaris G, Bouzakis E, Biermann D, M'Saoubi R. Cutting with coated tools: Coating technologies, characterization methods and performance optimization. CIRP Ann - Manuf Technol [Internet]. 2012;61(2):703–23. Available from: http://dx.doi.org/10.1016/j.cirp.2012.05.006
36. Junior EL. Assessment of Corrosion Behaviour of Machined Super Duplex Stainless Steel Obtained With Three Different Pvd Coated Tools Assessment of Corrosion Behaviour of Machined Super Duplex Stainless Steel Obtained With Three. McMaster University; 2019.
37. Sousa VFC, Silva FJG, Alexandre R, Pinto G, Baptista A, Fecheira JS. Investigations on the Wear Performance of Coated Tools in Machining UNS S32101 Duplex Stainless Steel. Metals (Basel). 2022;12(6).
38. Chowdhury MSI, Bose B, Rawal S, Fox-Rabinovich GS, Veldhuis SC. Investigation of the

wear behavior of pvd coated carbide tools during ti6al4v machining with intensive built up edge formation. Coatings. 2021;11(3):1–17.

39. Chowdhury MSI, Bose B, Yamamoto K, Shuster LS, Paiva J, Fox-Rabinovich GS, et al. Wear performance investigation of PVD coated and uncoated carbide tools during high-speed machining of TiAl6V4 aerospace alloy. Wear [Internet]. 2020;446–447(August 2019):203168. Available from: https://doi.org/10.1016/j.wear.2019.203168

40. Chowdhury MSI, Chowdhury S, Yamamoto K, Beake BD, Bose B, Elfizy A, et al. Wear behaviour of coated carbide tools during machining of Ti6Al4V aerospace alloy associated with strong built up edge formation. Surf Coatings Technol. 2017;313:319–27.

41. Raveendra S, Gustavsson F, Golpayegani A, Haraldsson J, Chai G. Microstructure analysis of segmented chips of super duplex stainless steel sandvik SAF 2507™ using electron microscopy techniques. Mater Perform Charact. 2017;6(3):456–65.

42. Pereira CBG, He Q, Soares P, Meruvia MS, de Souza GB, Amorim FL, et al. Tribological characterization of PVD TiSiN/AlCrN coating: A comprehensive study on thermal effect. Mater Charact [Internet]. 2023;203(April):113135. Available from: https://doi.org/10.1016/j.matchar.2023.113135

43. Vereschaka A, Grigoriev S, Sitnikov N, Aksenenko A, Milovich F, Andreev N, et al. Influence of the thickness of multilayer composite nano-structured coating Ti-TiN-(Ti,Al,Si)N on the tool life of metal-cutting tools and the nature of wear. Coatings. 2019;9(11):2–5.

44. He Q, Paiva JM, Kohlscheen J, Beake BD, Veldhuis SC. An integrative approach to coating/carbide substrate design of CVD and PVD coated cutting tools during the machining of austenitic stainless steel. Ceram Int. 2020;46(4):5149–58.

45. Beake BD, Fox-Rabinovich GS, Veldhuis SC, Goodes SR. Coating optimisation for high

speed machining with advanced nanomechanical test methods. Surf Coatings Technol [Internet]. 2009;203(13):1919–25. Available from: http://dx.doi.org/10.1016/j.surfcoat.2009.01.025